Quantifying the Statistical Relationships Between Flank Eruptions and Major Earthquakes at Mt. Etna Volcano (Italy)

Andrea Bevilacqua[1] , **Raffaele Azzaro[2]** , **Stefano Branca[2]** , **Salvatore D'Amico[2]** , **Franco Flandoli[3]** , and **Augusto Neri[1]**

[1]Istituto Nazionale di Geofisica e Vulcanologia, Sezione di Pisa, Pisa, Italy, [2]Istituto Nazionale di Geofisica e Vulcanologia, Sezione di Catania-Osservatorio Etneo, Catania, Italy, [3]Scuola Normale Superiore di Pisa, Pisa, Italy

Abstract At Mt. Etna volcano, flank eruptions are often accompanied by seismic swarms with damaging earthquakes; the most recent case-history is the 2018 flank eruption, associated with a destructive earthquake (M_w 5.0). In this paper, we analyze the earthquake and eruptive catalogs from 1800 to 2018, to produce quantitative estimates of the earthquake rate under the influence of flank eruptions. We quantify that 30% of the flank eruption onsets precede a major (i.e., damaging, $I_x \geq$ V–VI EMS) earthquake by 30 days or less; 18% of the major earthquakes follow a flank eruption onset in 30 days or less. Thus, we show that the probability of major earthquakes increases 5–10 times after the onset of flank eruptions and this effect lasts for 30–45 days. This is also observed after the end of the eruptions. Results indicate different relationships depending on the location of the volcano-tectonic systems considered individually (eruptive fissures, seismogenic faults). For instance, we describe a 10–20 times increased probability of earthquakes for 65–70 days after eruptions on the northeastern flank, and of new flank eruptions for 45–70 days after earthquakes of the Pernicana fault.

Plain Language Summary Historically, the flank eruptions of Mt. Etna have often been accompanied by destructive seismic events, although strong earthquakes have occurred during periods of volcanic quiescence too. As a result, the impact of both phenomena on local communities and territory is given by an alternation of two different hazards but still linked to each other. In this paper, by considering the up-to-date historical catalogs of earthquakes and eruptions at Mt. Etna, we quantify how probable it is, if compared to the average pattern, to have an earthquake temporally related to a flank eruption. That is, 30% of the flank eruption onsets precede a damaging earthquake by 30 days or less; the probability of strong earthquakes increases 5–10 times after the onset of flank eruptions and this effect lasts for 30–45 days. Thus, we show that the probability of damaging earthquakes drastically increases after the onset of flank eruptions and this effect lasts for several weeks. This is also observed after the end of the eruptions. Results provide the quantitative basis for a multihazard assessment that may enable better operative decisions to face future eruptive crises at Mt. Etna.

1. Introduction

Mount Etna (Italy) is the largest active volcano in Europe, and in the past 2,500 years, it has been characterized by an almost continuous activity at the summit craters and frequent eruptions from fissures along its flanks (Branca & Abate, 2019; Branca & Del Carlo, 2005; Figure 1). Flank eruptions represent the most dangerous type of eruptive activity at Etna, since they may occur close to vulnerable areas, such as towns, villages, lifelines, and cultivated land (Barberi et al., 1993, 2003; Branca et al., 2015a, 2017; Calvari & Pinkerton, 1998; Calvari et al., 1994; Del Negro et al., 2013, 2019; Favalli et al., 2009).

Typically, flank eruptions are accompanied by seismic swarms and, often, by destructive earthquakes, although strong events can occur during periods of volcanic quiescence too. As a result, the impact of both phenomena on the local population and their territory is given by an alternation of two different hazards but temporally, and in part also spatially, linked to each other.

Some studies dating back to the 1980–90s objectively identified the correlation between flank eruptions and damaging earthquakes, but their results were quantitatively affected by limitations in the historical catalogs considered, either in terms of short time periods, high macroseismic intensity thresholds, or outdated information (Azzaro & Barbano, 1996; Gresta et al., 1994; Nercessian et al., 1991; Sharp et al., 1981). Therefore, in this study, we improve on the previous results by analyzing the up-to-date historical catalogs of earthquakes and eruptions

Software: Andrea Bevilacqua
Supervision: Raffaele Azzaro, Augusto Neri
Validation: Andrea Bevilacqua, Franco Flandoli, Augusto Neri
Visualization: Andrea Bevilacqua
Writing – original draft: Andrea Bevilacqua
Writing – review & editing: Andrea Bevilacqua, Raffaele Azzaro, Stefano Branca, Salvatore D'Amico, Augusto Neri

at Mt. Etna. Our aims are: (a) to confirm and improve quantification of the probability of occurrence of damaging earthquakes given a flank eruption, and vice versa; (b) to better determine the persistence of the correlation between damaging earthquakes and flank eruptions; (c) to interpret these results in the framework of geophysical knowledge.

First, we provide an outline of the previous studies on the statistical link between flank eruptions and earthquakes at Mt. Etna (Section 2), and we describe our input data sets and their specific properties (Section 3). Then, we identify and quantify the statistical dependence of major earthquakes and flank eruptions (Sections 4 and 5), by considering two macroseismic intensity thresholds for the earthquakes (producing slight or severe damage), four spatial groups of eruptive fissures (Figure 1), and four systems of seismogenic faults (Figure 2). We also investigate the case of seismic events of the Pernicana fault preceding major seismicity in other fault systems. Finally, we discuss our methods and results (Section 6), point out their limitations and contextualize them with previous studies.

In summary, we analyze the interevent time distributions, estimate the rate of major earthquakes conditioned on the occurrence of a flank eruption, and constrain the duration of such statistical dependence. These findings are based on phenomenological observations reported in the historical catalogs, which, unlike instrumental data sets, do not include many geophysical parameters typically acquired by the monitoring networks. However, the probability rate of occurrence of earthquakes given flank eruptions represents a possible quantitative input to face multihazard scenarios during volcanic unrests and eruptive crises.

2. Statistical Analyses at Mt. Etna: Historical Background

Since the 1980–90s, the research on statistical relationships between flank eruptions and major earthquakes at Mt. Etna has been a debated topic to understand the behavior of the volcanic system as a whole. In the following, we briefly recall the main findings in this literature.

Sharp et al. (1981), by analyzing a data set of 49 flank eruptions and 620 earthquakes (with epicentral intensity $I_0 \geq$ V MCS) from 1582 to 1978, determined the nonhomogeneous Poisson distribution of flank eruptions and of 146 empirically selected mainshocks, by assuming variable Poisson rates equal to the 25-year average. They also performed a statistical test of independence between Poisson processes based on event counting of flank eruptions in time windows left-anchored to the mainshocks (Cox, 1955; Cox & Lewis, 1966; Morley & Freeman, 2007; Niehof & Morley, 2012), and identified a statistically significant relationship between the onset of flank eruptions and the prior occurrence of mainshocks. Nercessian et al. (1991) reanalyzed the catalogs of Sharp et al. (1981) and changed the mode of mainshock selection, increasing the data set to 160 mainshocks. By applying the statistical test of Cox (1955), they deduced that both the onset and end of flank eruptions are likely followed by mainshocks, i.e., an opposite event sequence to the one identified by Sharp et al. (1981). Our results confirm this conclusion.

Gresta et al. (1994) found a statistical correlation between the seven largest Etna earthquakes ($I_0 \geq$ IX MCS) and the end of the 40 main eruptions, flank, and summit ones, with volumes $\geq 10^7$ m³, in the time span 1600–1989. They tested the Spearman ranking coefficient (Conover, 1980), obtained on a 30-day window after eruptions end, i.e., three associations over seven eruptions. They also identified a weaker correlation in the 30 days before the eruptions onset, i.e., only one observed association, and they could not reject the null hypothesis of independence in this case. It is worth noting that the data sets of Gresta et al. (1994) were considerably different from those adopted by previous studies, and by us, therefore a comparison is not straightforward.

With the installation of the first seismic network in the late 1970s and the increasing collection of instrumental seismic data (Scarpa et al., 1983) several studies shifted attention toward decade-long analyses (e.g., Cardaci et al., 1993; Mulargia et al., 1991, 1992). Among them, Gasperini et al. (1990) analyzed 1,458 seismic events ($M_d \geq 2.8$) and nine flank eruptions during the decade 1978–1987, not finding any relationship between the series of events because of the scarcity of data. By contrast, Mulargia (1992) identified 12 seismic sequences in 1974–1991, and compared them with 11 flank eruptions by means of a Poisson independence test based on event rates rather than event counting (intensity cross-product, Brillinger, 1976). Therefore, he concluded that flank eruptions are precursors of seismic sequences. However, all these studies considered significantly different data
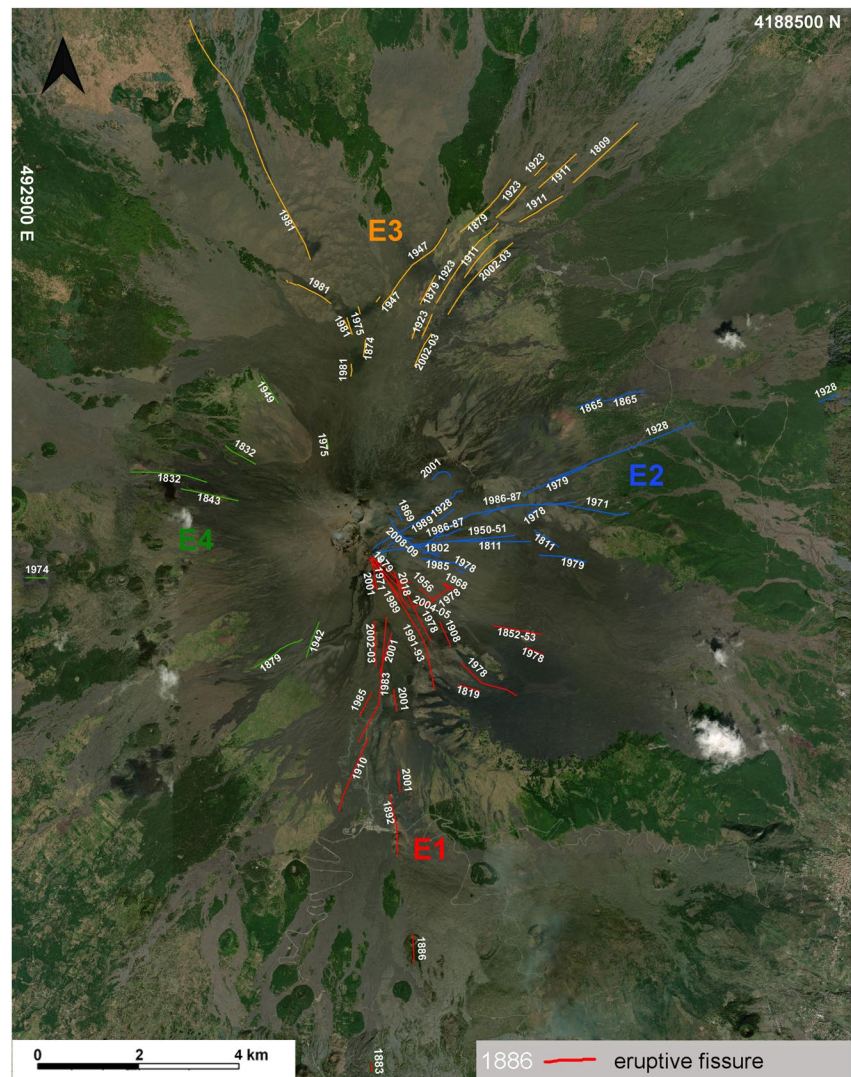
Figure 1. Mt. Etna overview of eruptive fissures of flank eruptions from 1800 to 2018. Different colors correspond to the different spatial groups, E1–E4. Labels show the year of the events. The GIS shapefiles of eruptive fissures are attached in Data Set S3 in Supporting Information S1. UTM WGS84, Zone 33N coordinate system.

sets from the historical catalogs, namely a rather small number of flank eruptions and major earthquakes but a larger number of seismic events of small magnitude.

In the following years, the huge amount of data produced by the seismic network allowed focusing on pattern recognition analyses, typically on the small earthquakes preceding flank eruptions (Bonaccorso et al., 2004; De Rubeis et al., 1997; Gresta & Longo, 1994; Latora et al., 1999; Neri et al., 2005; Sandri et al., 2005; Vinciguerra et al., 2001). These results highlighted interesting connections between earthquakes and eruptions, but they focused on eruption forecasting rather than on the occurrence probability of damaging earthquakes, and the statistical studies of the 1980–90s have not been updated since then.

3. Input Data: The Historical Catalogs of Mt. Etna

Past activity of Mt. Etna is well documented by numerous historical sources that, since the late 16th century, report accounts, descriptions, and iconographies on the volcanic and seismic phenomena occurring on the volcano. Such a large data set of historical information is not frequent worldwide but is comparable, in Italy, to that of Vesuvius, although the frequency of eruptions and earthquakes for this volcano is much lower than at Etna.

Figure 2. Mt. Etna overview of active faults and historical damaging earthquakes, i.e., with maximum intensity $I_x \geq$ V–VI EMS, from 1800 to 2018. Labels show the year of the greatest earthquakes, i.e., with $I_x \geq$ VII–VIII EMS. Different colors correspond to the different systems of faults, F1–F4. Fault lines are from Azzaro et al. (2012b). UTM WGS84, Zone 33N coordinate system.
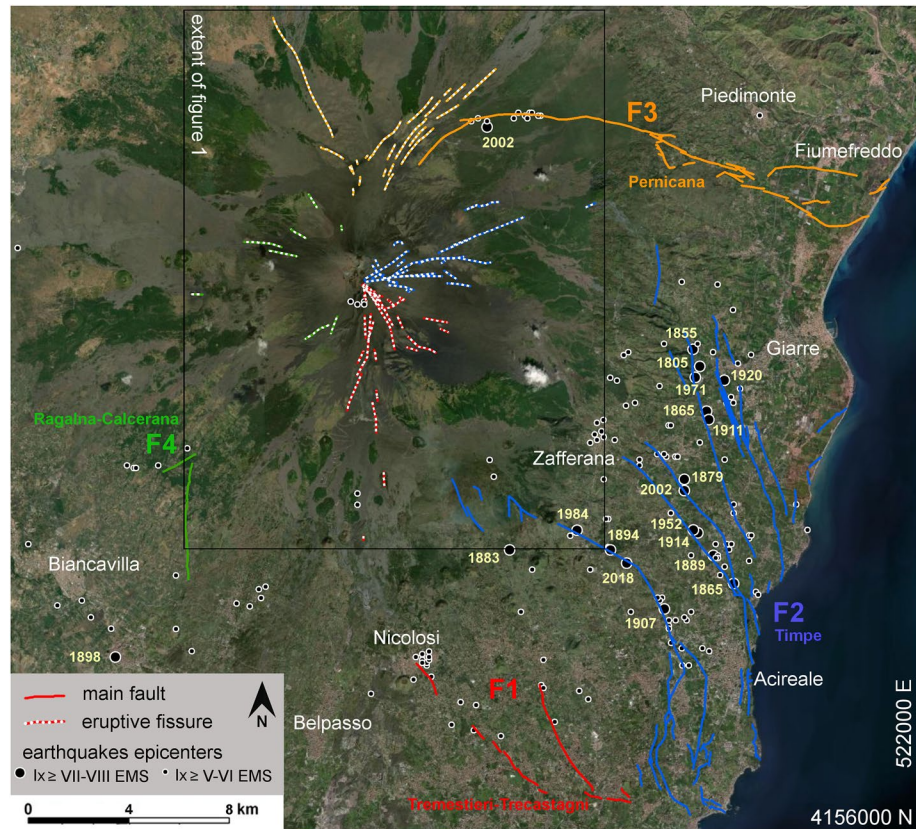
3.1. The Catalog of Volcanic Eruptions

3.1.1. Overview and Applications

The International Association of Volcanology and the Smithsonian Institution promoted the first modern catalogs of Mt. Etna volcanic activity (Imbò, 1965; Simkin, 1981). Later, more detailed historical records were published, including critical analyses of ancient documents and a re-examination of literature data (Chester et al., 1985; Romano & Sturiale, 1982; Tanguy, 1981; Wadge, 1977). Then, Branca and Del Carlo (2004, 2005) produced an updated and significantly improved catalog whose data set of flank eruptions was as complete as possible for the past 400 years. They indicated that, during the period from 1600 to 1975, the eruption frequency and lava output of Etna were relatively uniform, while since 1975 they increased markedly. Other catalogs have since been published without substantial changes in the flank eruption records, but enhancing the scientific reconstruction of the past and recent activity from different perspectives (Andronico & Lodato, 2005; Behncke et al., 2005; Neri et al., 2011; Tanguy et al., 2007). More recently, Branca and Abate (2019) further detailed the historical catalog before the 18th century by a multidisciplinary approach comprising stratigraphy, historiographical studies, and geochronological dating of the lavas, that allowed defining a comprehensive assessment of the flank eruptions at Etna in the last 2500 years (Branca & Vigliotti, 2015; Branca et al., 2011, 2013, 2015b, 2016; Tanguy et al., 2012).

At the same time, a number of statistical analyses of Mt. Etna eruption records were undertaken in order to characterize the eruptive behavior of Etna. Wickman (1976) first analyzed the historical eruption record in terms of annual rate of occurrence, seeking for patterns in the eruptive behavior and not finding change points.

Mulargia et al. (1985) stated that the flank eruption times from 1600 to 1980 are stationary, randomly distributed with a constant rate, i.e., following a homogeneous Poisson process. A few years later, however, Mulargia et al. (1987) changed this conclusion claiming that the interevent time of flank eruptions in the period 1600–1980

actually followed two distinct regimes before and after year 1865, while the eruptive activity in the period 1971–1981 followed four different regimes. The reason for this revision was that a Kolmogorov-Smirnov test evaluates the entire distribution of interevent times regardless of their sequence, thus in the older paper that test was not sensitive to change points in the Poisson rate. Ho (1991) first fitted a Weibull process to the cumulative onset times of flank eruptions, and found moderate evidence against the homogeneous exponential hypothesis, and then Ho (1992) further detailed a Poisson change-point identification algorithm.

Salvi et al. (2006) fitted a parametric model for the rate function of a nonhomogeneous Poisson process which allowed its variation as a power function of time. They claimed strong statistical evidence for an increasing number of flank eruptions after 1980. Bebbington (2007) compared various statistical models for flank eruptions at Mt. Etna in terms of hidden Markov chains—the volcanic system was assumed to switch between a number of states with different eruption rates, but the preferred models were all Poisson in their prevalent state. He identified possible change points in 1611, 1971, 1991, 2001 for two-state models.

Smethurst et al. (2009) analyzed the up-to-date catalogs of Branca and Del Carlo (2005) and Tanguy (2007). They concluded that flank eruptions at Etna between 1610 and 2008 follow an inhomogeneous Poisson process, with intensity of eruptions increasing almost linearly since the mid-1900s, without identifying any cyclical pattern over this period. Cappello et al. (2013) implemented a nonhomogeneous Poisson process with space-time varying rates and found evidence of spatial nonhomogeneity and temporal nonstationarity of flank eruptions, confirming a general increase in the eruptive frequency starting from 1971.

In our analysis, we adopt a nonhomogeneous Poisson process with rate equal to a 25-year average of the data, i.e., what we called a Poisson process with "slowly varying" rate. This approach is capable of describing the past observed rate changes consistently with the previous statistical analyses.

3.1.2. Statistical Description

The catalog used in this study is from Branca and Del Carlo (2005), updated with information from the weekly Bulletins of INGV (https://www.ct.ingv.it). It also includes a critical revision of the location of eruptive fissure/vents, as described in Section 5. We considered the period from 1600 to 2018, a significantly wide time span with regard to the occurrence of flank eruptions. Data Set S1 in Supporting Information reports this data set. The comparison to other catalogs is beyond the scope of this paper, but we stress that this data set represents an as complete as possible and homogeneous data set of flank eruptions in the last four centuries (Neri et al., 2011; Tanguy et al., 2007).

Figure 3a shows the cumulative count of flank eruptions—68 events in total, of which $49/68 = 72\%$ occurred after 1800. Since 1800 we marked the $26/49 = 53\%$ events that had their onset or end in ±4 months from a major earthquake (i.e., damaging). Note that this ±4 months interval only has a descriptive purpose and we are not hypothesizing that it may be the actual duration of statistical dependence of the two phenomena. Figure S10 in Supporting Information S1 summarizes the flank eruption durations, showing a significant variability from 1 day to about 1.5 years after 1700, and even longer durations in the 17th century; nevertheless, having reliable observations about the eruptions end becomes challenging for the older events (Branca & Abate, 2019). We note that $10/68 = 15\%$ events, and $8/49 = 16\%$ after 1800, have been characterized by having eruptive fissures above 2,850 m, directly propagating from one of the summit craters—we marked them as "subterminal eruptions" (e.g., the 2008–2009 eruption; Alparone et al., 2012; Bonaccorso et al., 2011). We consider them in our catalog and test their sensitivity in Section 5.1.

Figure 3b plots the annual flank eruption rate, either obtained on a left-side moving window of 10 and 25 years (Bevilacqua et al., 2016, 2018, 2020). The graphs clearly evidence the rate gap in the first half of 18th century, and the anomalous rate peak after 1971, with a peak of 1 event/year in the 10-year average, apparently concluded after 1990. The average rate from 1600 to 2018 is one event every 6.2 years; one event every 4.5 years after 1800. Figure S10 in Supporting Information S1 shows the histogram of interevent times, i.e., from each onset to the next onset, of flank eruptions after 1600, characterized by 140 days at 5th percentile, 550 days at 20th percentile, ~4 years at 50th percentile, and ~15 years at 90th percentile.

Figure 3c plot the staircase graph of the Poisson test of Cox (1955), by considering the flank eruptions onset. Figure S10 in Supporting Information S1 shows a similar graph for flank eruptions end. In particular, the discrete
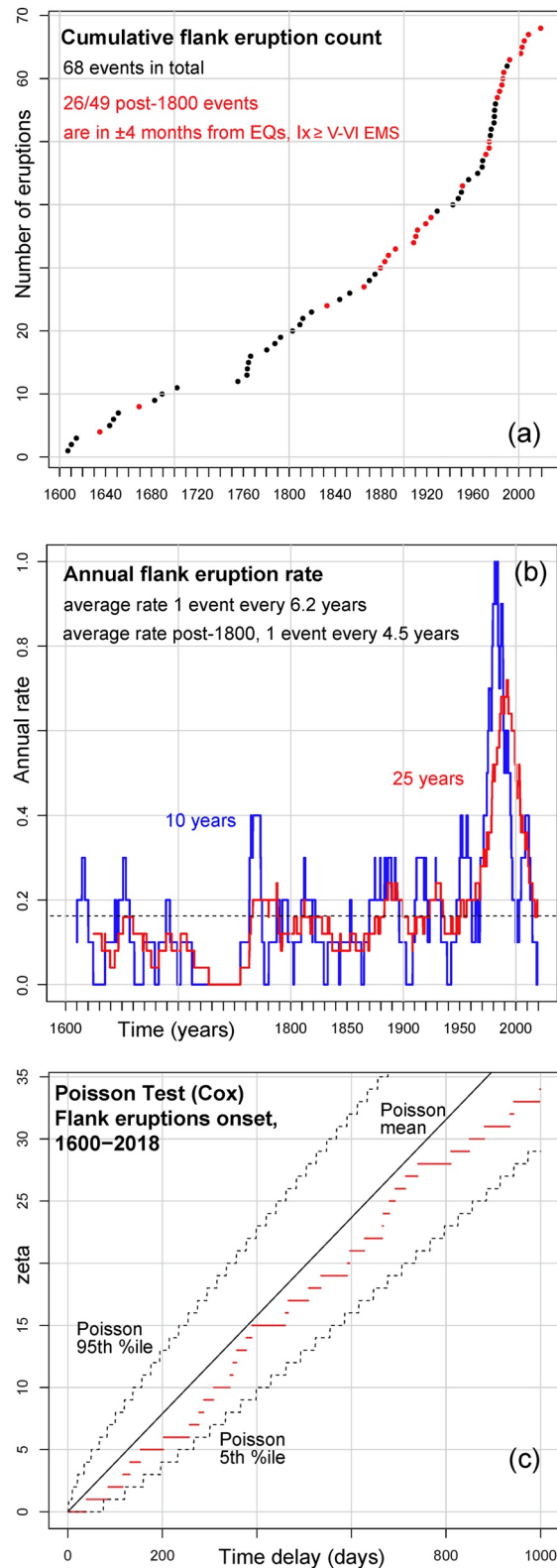
Figure 3. Statistical description of the flank eruptions records from 1600 to 2018. (a) The cumulative count of flank eruptions, with those ±4 months from major earthquakes marked in red. (b) The annual rate, using either 10-year (blue) and 25-year (red) moving windows. The average rate is indicated with a dashed line. (c) The test of Cox (1955) comparing the clustering properties of eruptions onset with those of a Poisson process. In Figures S10 and S11 in Supporting Information S1, we include the same test on the eruptions end, and on the eruptive record from 1800 to 2018. The colored lines are the real data.

variable ζ counts the total number of occurrences of new events in right-side time windows after all events in the series, except the last, as a function of the size Δt of the windows

$$\zeta(\Delta t) = \sum_{j=1}^{n-1} N(aj, \, aj + \Delta t) \tag{1}$$

where $N(t_1, t_2)$ is the number of events in $(t_1, t_2]$, and $(a_j)_{j=1,\dots,n}$ is the considered sequence of events. If $(a_j)_{j=1,\dots,n}$ is generated by a Poisson process, then the discrete variable ζ is Poisson-distributed with an average value

$$E[\zeta(\Delta t)] = n(n-1)\Delta t \, / T \tag{2}$$

where T is the total duration of the record considered. The test is generalized to a nonhomogeneous case by decomposing the time interval in k 25-year long subintervals $(I_i)_{1,\dots,k}$, and defining

$$\zeta(\Delta t) = \sum_{i=1}^{k} \zeta_i(\Delta t) \tag{3}$$

where for all i in $1, \dots, k$, $\zeta_i(t)$ is defined inside I_i (Sharp et al., 1981). This test confirms that both the time series of flank eruptions onset and end are compatible with a nonhomogeneous Poisson process with rate equal to a 25-year average of the data, i.e., a Poisson process with "slowly varying" rate.

3.2. The Macroseismic Catalog of Earthquakes

3.2.1. Overview and Applications

Seismic activity at Mt. Etna is documented through two types of catalogs, the historically derived data sets based on macroseismic data and the instrumental catalogs, listing a large number of events also of small magnitude but for shorter time spans. In our study, we considered the first typology of catalogs, since they cover significantly broader time spans (hundreds of years), more suitable for long-term statistical analyses; on the other hand, they report events above a significant magnitude threshold, which produced important macroseismic effects (i.e., damage).

In the 1970–90s, the earthquakes of the Etna region were included in the catalogs of the Italian seismicity (Boschi et al., 1995, 2000; Camassi & Stucchi, 1997; Carrozzo et al., 1975; Gruppo di Lavoro CPTI, 1999; Postpischl, 1985), but in each of them the volcano-related seismicity appeared rather fragmented and not consistent from one catalog to another. In practice, these catalogs mostly reported the largest events—epicentral intensity $I_0 >$ VIII in the Mercalli-Cancani-Sieberg scale (MCS)—and they have significant problems of completeness, thus representing Etna's seismicity inadequately.

For this reason, Azzaro et al. (2000), by exploiting the highly informative potential of the historical sources, compiled a specific catalog of the Etnean earthquakes (hereinafter CMTE), which includes foreshock and aftershock and provides a homogeneous and not declustered data set of earthquakes, allowing investigating the space-time evolution of seismic sequences and the possible relationships with the eruptive activity. The CMTE catalog is regularly updated, the current issue covering the time span from 1600 to 2018 (Azzaro & Castelli, 2015; Azzaro & D'Amico, 2019). These characteristics led the CMTE to be adopted as the main reference source of data for the Etna region in the framework of the Italian earthquake catalog CPTI issued by INGV (Rovida et al., 2020). Data Set S2 inSupporting Information S1 reports our analyzed version of the CMTE, listing 1,818 events in total. It is worth noting that in the CMTE catalog intensities are assessed by the European Macroseismic Scale 1998 (EMS, see Grünthal, 1998), but these estimations are consistent with the MCS values (Musson et al., 2009).

One of the main issues in analyzing historical earthquake data sets is the definition of the magnitude for the preinstrumental period. The problem is classically solved by using empirical relationships between macroseismic intensity and magnitude; as for Etna, the most recent set of relationships specific for this volcanic region is from Azzaro et al. (2011), who derived different I-M regressions calibrated on duration magnitude M_d, local magnitude M_L, and moment magnitude M_w. However, since we found that the calculation of the macroseismic magnitude may prove underestimated in some particular cases (e.g., deep earthquakes, events located far from inhabited areas), we preferred to use the maximum intensity I_x, which is a parameter directly referring to the earthquake's

impact on the territory (Azzaro et al., 2008). For the sake of clarity, Data Set S2 in Supporting Information S1 also reports the different estimations in the aforementioned magnitude scales. Lastly, we note that the catalog also indicates the association of stronger events with the causative fault, based on the occurrence of coseismic surface ruptures (Azzaro, 1999).

In conclusion, while CMTE has been used to improve the knowledge of long-term seismicity and seismotectonics (Azzaro et al., 2012a, 2013b, 2020), and to assess seismic hazard at the scale of the volcano (Azzaro et al., 2013a, 2016, 2017), previous analyses integrated with the eruptive activity are limited to a few case studies (e.g., Azzaro & Barbano, 1996; Azzaro et al., 2001).

3.2.2. Statistical Description

In our analysis, we focus on a subset of data from the CMTE catalog, only considering the earthquakes having an impact in terms of seismic hazard, i.e., those causing damage to buildings. This typology of events, characterized by very shallow hypocenters and a strong intensity attenuation determining small damage areas (Azzaro et al., 2006), is historically well documented given the dense urbanization of the volcano's flanks. More specifically, we focused on two thresholds of macroseismic intensity, $I_x \geq$ V–VI and $I_x \geq$ VII–VIII EMS, corresponding to slight and severe-heavy damage, respectively (Grünthal, 1998). The completeness of this data set decreases before the 19th century, so we focused on the time span 1800–2018. More details are in Sections 5.2 and 5.3.

Figures 4a and 4b show the cumulative count of earthquakes with $I_x \geq$ V–VI EMS—171 events in total, and with $I_x \geq$ VII–VIII EMS—19 events in total. We marked the 85/171 = 50% events in Figure 4a and 10/19 = 53% events in Figure 4b that occurred in ±4 months from a flank eruption onset or end. Note that this ±4 months interval has a descriptive purpose only (see Section 4 for more details).

Figures 4c and 4d plot the annual earthquake rate, for the two intensity thresholds, either obtained on left-side moving windows of 5, 10, and 25 years (Bevilacqua et al., 2016, 2018, 2020). In Figure 4c, the graphs clearly show two 40-year-long rate increases in 1880–1920 and in 1970–2010, both characterized by a bimodal profile with maximum rates at the beginning and at the end. The second-rate increase is greater than the first one and in 1985 it reached 7 events/year with $I_x \geq$ V–VI EMS, according to the 5-year average. Their average rate is one event every 1.3 years from 1800 to 2018.

In Figure 4d, the 40-year-long rate increases are less evident, but still observable with some differences. The first-rate increase is greater than the second one and before 1920 it reached 0.3 events/year with $I_x \geq$ VII–VIII EMS, in a 10-year average. Their average rate is one event every 11.5 years from 1800 to 2018.

Figures 4e and 4f plot the staircase graph of the Poisson test of Cox (1955), considering 106 mainshocks with $I_x \geq$ V–VI and 17 mainshocks with $I_x \geq$ VII–VIII EMS, respectively. This test has been described in Section 3.1.

We selected the mainshocks through this empirical selection algorithm:

(i) delete all the earthquakes in a right-side window after each other earthquake in the catalog, according to the following formula defining the window length

$$\tau\,(I_x) \;:=\; 10^{0.65\,+\,0.185\,Ix} \tag{4}$$

thus τ(V–VI) = 47 days, τ(VII–VIII) = 110 days;

(ii) reinsert the event of maximum intensity in each window considered, if that was not the first in the sequence;
(iii) delete the events with lower magnitude if two or more events occurred in <1 day.

In detail, (i) is from Sharp et al. (1981), (i + ii) is from Nercessian et al. (1991), and we added (iii) to correct a slight excess of events with very short time intervals.

Neither of the two considered time series is characterized by clusters of periodicity that differ from a Poisson process with "slowly varying" rate, i.e., equal to a 25-year average of the data. The Poisson properties of both the flank eruptions and the mainshock enables the application of the test of independence of Cox (1955), as implemented in Sharp et al. (1981). The test provides statistical evidence that the earthquakes with either $I_x \geq$ V–VI or $I_x \geq$ VII–VIII EMS are not independent from either the flank eruption onsets or ends. This result is further detailed in Figures S12 and S23 in Supporting Information S1.
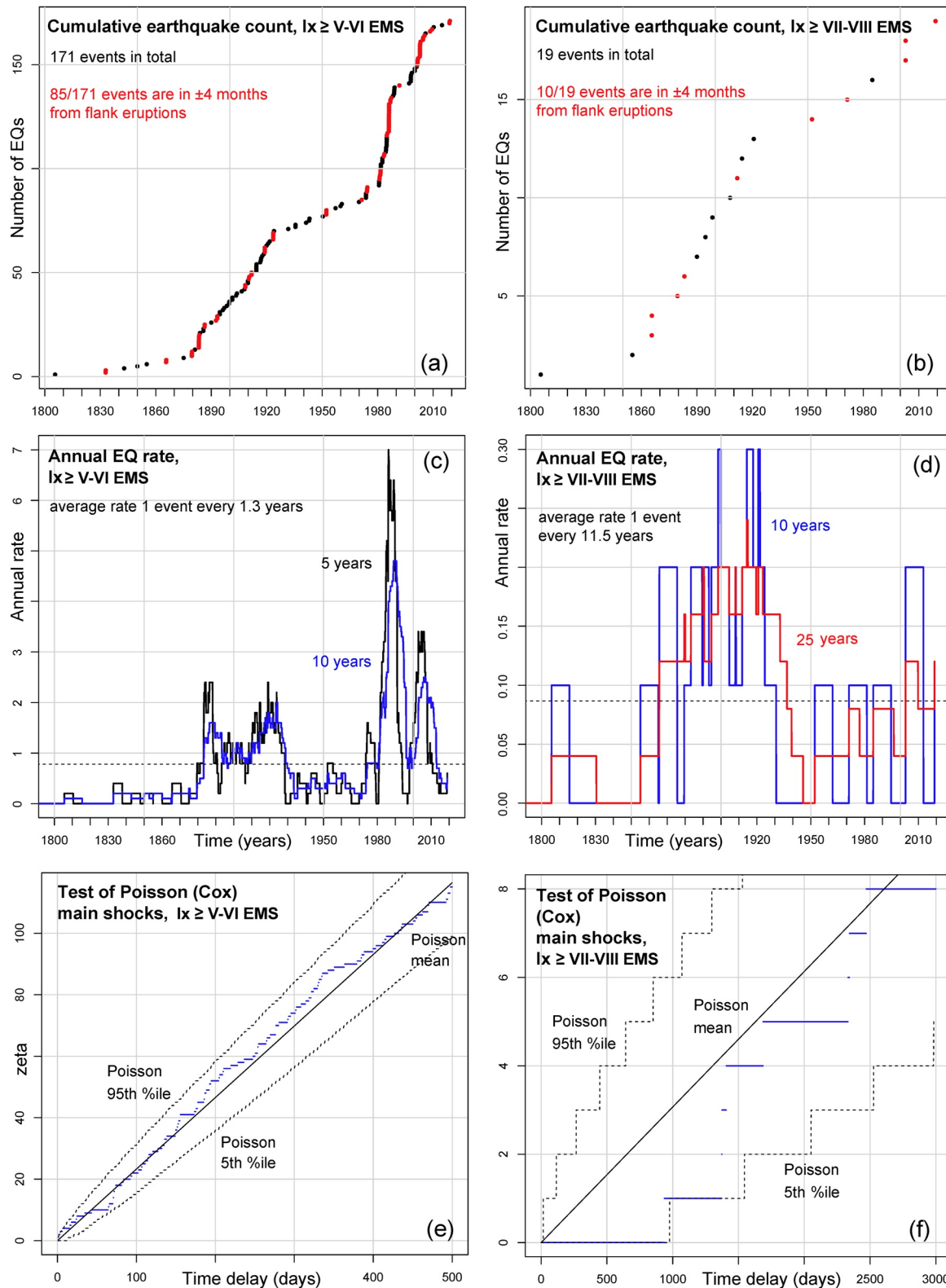
Figure 4. Statistical description of the major earthquakes record from 1800 to 2018, (a, c, e) $I_x \geq$ V–VI, (b, d, f) $I_x \geq$ VII–VIII EMS. (a, b) The cumulative count of earthquakes, marking in red those ±4 months from flank eruptions. (c, d) The annual rate, either using 5-year (black, only in c), 10-year (blue), and 25-year (red, only in d) moving windows. The average rates are reported with a dashed line. (e, f) The test of Cox (1955) comparing the clustering properties of mainshocks, with those of a Poisson process. The colored lines are the real data.

We should add that the following analysis does not rely on this test, but it directly quantifies the interevent time distributions and the conditional rates of damaging earthquakes.

4. Global Statistical Analysis of Interevent Time Between Flank Eruptions and Earthquakes

The key data set that defines the relationship between flank eruptions and major earthquakes is the interevent time, i.e., the family of all time differences between the two data sets. This set generalizes the interevent time of a single sequence of events (i.e., Bevilacqua et al., 2018, 2020), and has a cardinality equal to the product of the two data sets. We focus our plots on the interevent times lower than 4 months—this choice only defines the considered domain and does not affect our results. Note that a 4-month time span is significantly longer than the observed correlation. Nevertheless, this choice prevented us from repeatedly counting the interevent times of the same earthquake with respect to more than one eruption.

4.1. Cumulative Probability Distribution of Minimum Interevent Time

In the following, we present the cumulative distribution of the interevent time in various cases: Figure 5 focuses on the case of damaging earthquakes following flank eruptions, Figures S13 and S24 in Supporting Information S1 count all the associations of major earthquakes and eruptions, i.e., regardless of their ordering. This section only considers the minimum interevent time for each phenomenon, i.e., consecutive occurrences. We further detail this in Sections 4.2 and 4.3, by extending the analysis to all the interevent times, and not just the minimum interevents.

In particular, Figures 5a and 5c focus on the cumulative probability of flank eruptions that occurred less than k days preceding a major earthquake. This probability is defined as $P^{(1)}(k, (a_i), (b_j))$, $\forall k \in \{1, \ldots, 120\}$, where

$$P^{(1)}(k, (a_i), (b_j)) := |\{a_i : min_j [(b_j - a_i) : b_j > a_i] < k\}|/|\{a_i\}| \qquad (5)$$

About 30% of the flank eruption onsets and 17% of flank eruption ends preceded an earthquake with $I_x \geq$ V–VI EMS of 30 days or less, respectively. In addition, about 9% of the flank eruption onsets and 7% of ends preceded an earthquake with $I_x \geq$ VII–VIII EMS of 30 days or less.

Then, Figures 5b and 5d express similar cumulative probabilities in terms of major earthquakes. That is

$$P^{(2)}(k, (a_i), (b_j)) := |\{b_j : min_j [(b_j - a_i) : b_j > a_i] < k\}|/|\{b_j\}| \qquad (6)$$

$\forall k \in \{1, \ldots, 120\}$. In this case, about 18% of the earthquakes with $I_x \geq$ V–VI EMS and 21% of those with $I_x \geq$ VII–VIII EMS followed in 30 days or less a flank eruption onset; 10% and 16% followed a flank eruption end.

Under the assumption of not overlapping windows, the union of all the intervals of 30 days can be compared to the average rate of one mainshock with $I_x \geq$ V–VI EMS every 2.1 years, providing a percentage of covered time equal to ~4%. Instead, the average rate of an eruption every 4.5 years would produce percentages of covered time equal to ~1.8%. Thus, the percentages observed in Figure 5 are all significantly greater than those that could be explained by independent phenomena.

For the sake of completeness, in Figure S14 in Supporting Information S1, we show the opposite case, i.e., a damaging earthquake preceding a flank eruption. This highlights a brief increase in the number of earthquakes, limited to 1–10 days preceding the eruption. All percentage values described in this section are summarized in Table S8 in Supporting Information S1.

4.2. Histograms of Interevent Time

Figure 6 reports the histograms of the interevent time of earthquakes and flank eruptions <4 months, including the pie charts of the positive and negative values. These graphs only describe the distribution of interevent times in [−120, 120] days, and they are not representative of all the earthquakes in the catalog. In Data Set S4 in Supporting Information S1, we include examples based on ±2 months that lead to equivalent results.
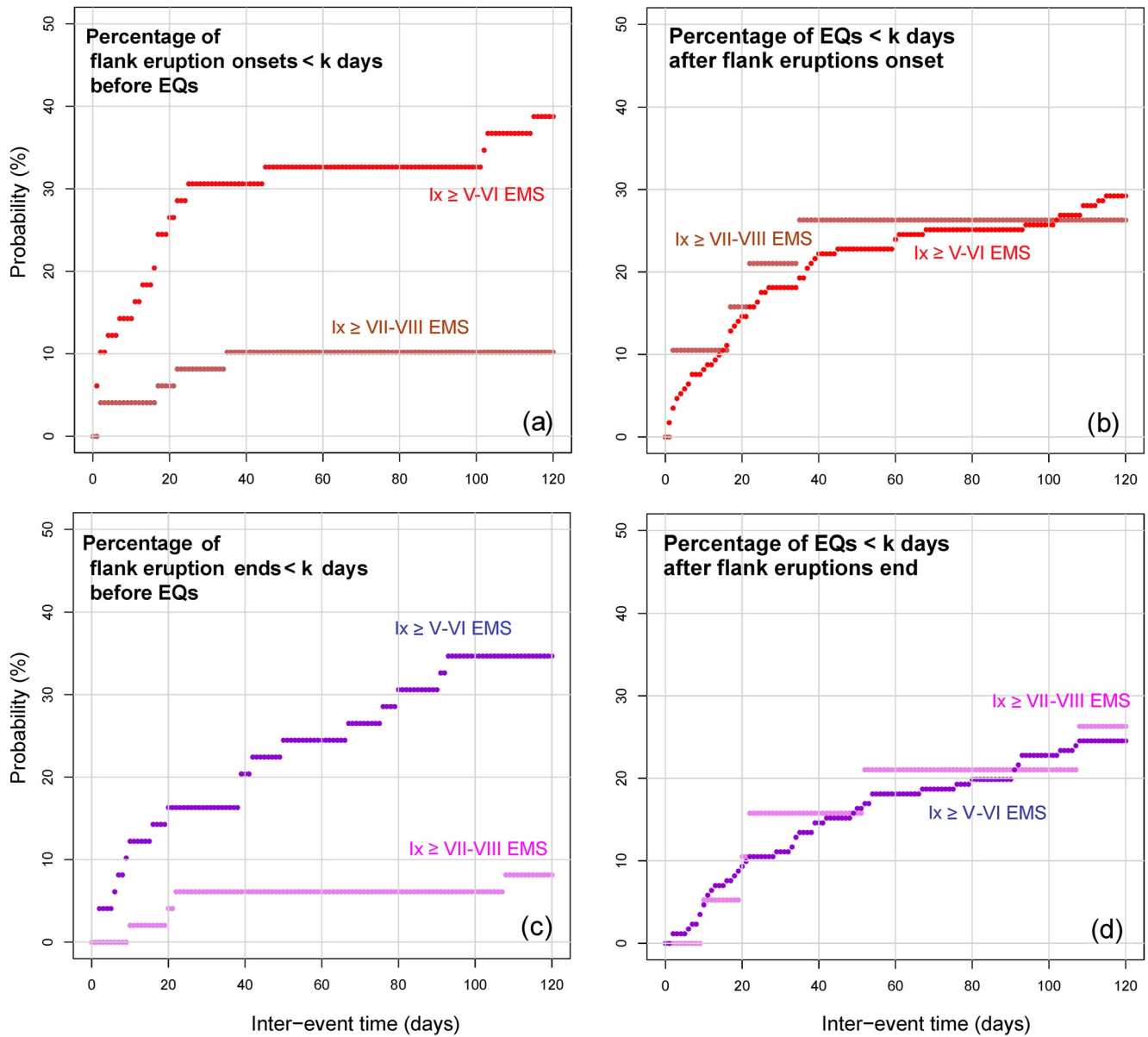
Figure 5. Statistical description of the cumulative probability of flank eruptions and major earthquakes, with respect to their minimum interevent time. We show the percentage of (a, c) flank eruptions preceding earthquakes and of (b, d) major earthquakes following flank eruptions. (a, b) Consider the onset of flank eruptions, while (c, d) the end. Figures S13 and S24 in Supporting Information S1 show the percentage of flank eruptions and major earthquakes either preceding or following by k days or less the other type of phenomenon.

Figures 6a and 6b consider the interevent time statistics between flank eruptions onset and the earthquakes, below the ±4 months' threshold. In particular, 67% of the earthquakes with $I_x \geq$ V–VI EMS followed the eruption onset and another 12% preceded it by <2.5 days; 71% of the earthquakes with $I_x \geq$ VII–VIII EMS followed the eruption onset, and all the others preceded it by <2.5 days.

Figures 6c and 6d consider the interevent time statistics between flank eruptions end and earthquakes, below the ±4 months' threshold. In particular, 54% of the earthquakes with $I_x \geq$ V–VI EMS followed the eruption end; 50% of the earthquakes with $I_x \geq$ VII–VIII EMS followed the eruption end.

However, as mentioned above, several earthquake occurrences preceding the eruption end are almost contemporaneous with the eruption onset, e.g., in 2002–2003, 1883, 2018. So, Figures 6e and 6f show the same statistics of Figure 6c, but excluding the earthquakes that occurred ±2.5 days from the flank eruptions onset. This
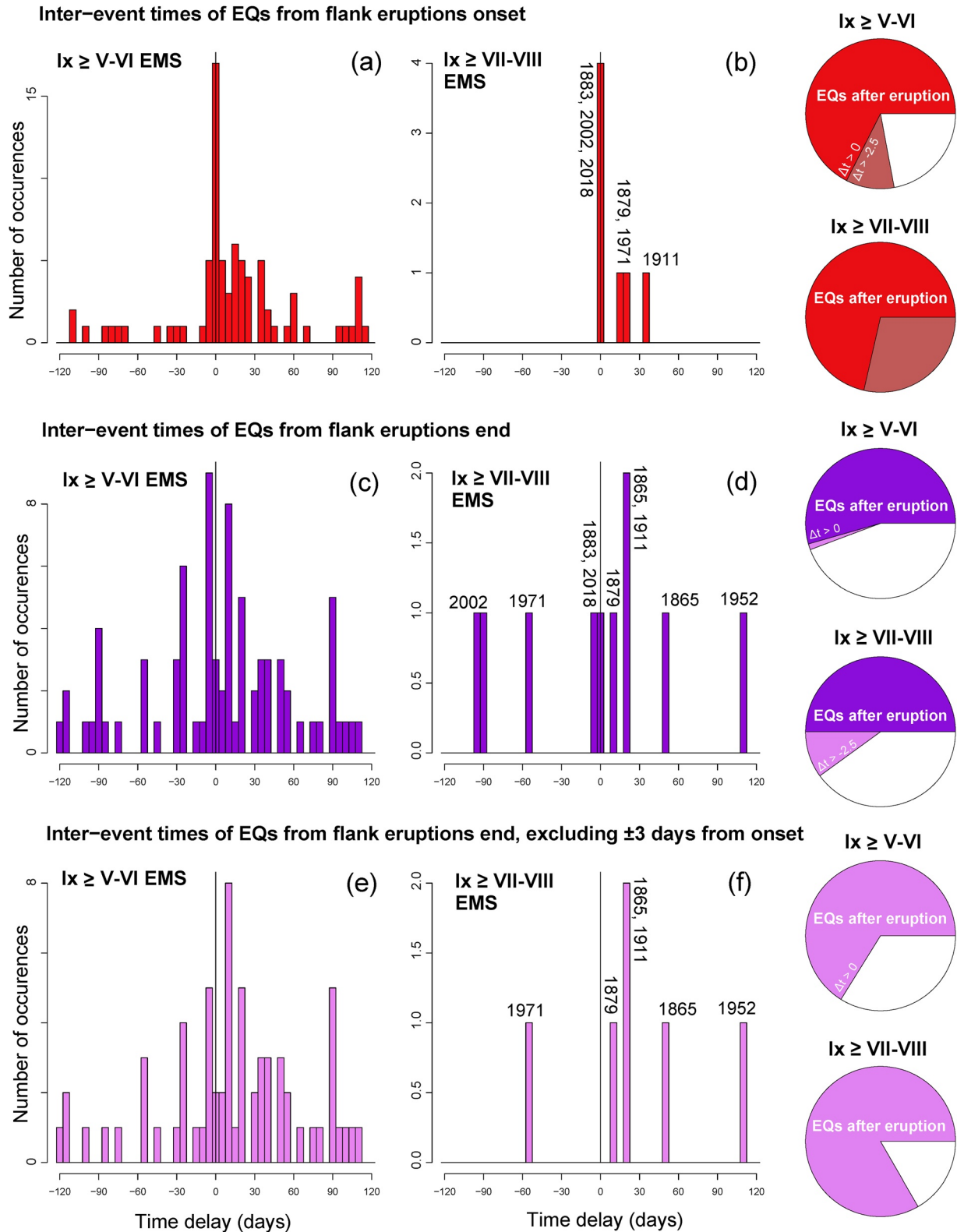
Figure 6. Histograms of the interevent time of earthquakes and flank eruptions <4 months, including pie charts of the positive values (dark colors), negative values in [−2.5, 0] days (light colors), and lower than −2.5 days (white). (a, c, e) show the earthquakes with $I_x \geq$ V–VI EMS; (b, d, f) those with $I_x \geq$ VII–VIII EMS. (a, b) Consider the flank eruptions onset (red); (c–f) consider the flank eruptions end (purple and pink). (e, f) Exclude the earthquakes occurring ±2.5 days from the onset.

significantly strengthens the skewness of the distribution below the ± 4 months' threshold, thus 66% of the earthquakes with $I_x \geq$ V–VI EMS followed the eruption end; 83% of those with $I_x \geq$ VII–VIII EMS followed the eruption end.

4.3. Conditional Rate of Major Earthquakes

Figure 7 reports the conditional rate λ of the earthquakes $(b_j)_{j=1,...,n2} < \pm 4$ months from flank eruptions $(a_i)_{i=1,...,n1}$. The rate $\lambda(t)$ is defined by the following formula:

$$\lambda(t) := \sum_{i=1}^{n1} N(a_i + t - dt,\ a_i + t) / (dt \cdot n1),\ \forall\ t\ \epsilon\ \{dt, \ldots, 120\} \tag{7}$$

$$\lambda(t) := \sum_{i=1}^{n1} N(a_i,\ a_i + dt)/(dt \cdot n1),\ \forall\ t\ \epsilon\ \{0, \ldots, dt\}$$

$$\lambda(t) := \sum_{i=1}^{n1} N(a_i - dt,\ a_i)/(dt \cdot n1),\ \forall\ t\ \epsilon\ \{-dt, \ldots, 0\}$$

$$\lambda(t) := \sum_{i=1}^{n1} N(a_i + t,\ a_i + t + dt)/(dt \cdot n1),\ \forall\ t\ \epsilon\ \{-120, \ldots, -dt\},$$

where $N(t_1, t_2)$ is the number of events $(b_j)_{j=1,...,n2}$ in (t_1, t_2), and dt is a bandwidth parameter.

This formula is inspired by the variable ξ in the test of independence of Cox (1955), and quantifies the earthquake rate in the days preceding or following a flank eruption. For all $t\ \epsilon\ \{-120, \ldots, 120\}$, $\lambda(t)$ estimates the sum of earthquakes inside dt-wide moving windows placed t days from every flank eruption, divided by the sum of the length of these windows. In Figure 7, we assume $dt = 10$ days, and in Data Set S5 in Supporting Information S1, we report the results when $dt = 5$ days, showing that the choice of dt does not significantly affect our description of data.

The profile of the conditional rate plots closely resembles, by construction, the histograms of interevent times; they thus communicate the same information in terms of expected annual rate of the events, rather than in terms of interevent time probability of occurrence. However, in addition to the histograms, the conditional rate also includes the information of the percentages in Figure 5 and Table S8 in Supporting Information S1.

Some of the gaps and peaks that we go on to describe in the conditional rates may be related to the small number of samples considered, especially in Section 5. Therefore, they are not always significant of an actual rate change. For example, under the assumption of a Poisson rate θ in the analyzed interval, the probability P_h of observing a gap of width h would be

$$P_h \leq exp(-\theta h)^{\check{N}} \approx exp(-N\check{N}h/T\check{N}) = exp(-Nh/T) \tag{8}$$

where N is the total number of earthquakes observed, T is the time interval of analysis, and $\check{N}$ is the number of eruptions considered. Here, we approximated $\theta \approx N/T\check{N}$. This equation tells us that the statistical significance of a gap of width h is related to the number N, i.e., $P_h < 0.05$ if $N > 3\ T/h$. In more detail, if $N(h) := 3\ T/h$ and $T = 4$ months, we have $N(10\ \text{days}) = 36$, $N(15\ \text{days}) = 24$, $N(20\ \text{days}) = 18$, $N(30\ \text{days}) = 12$, $N(40\ \text{days}) = 9$. Figure 7 includes the number N before and after the eruption onset and end.

In detail, Figures 7a and 7b consider the flank eruptions onset and the earthquakes with (a) $I_x \geq$ V–VI and (b) $I_x \geq$ VII–VIII EMS. In plot (a), the conditional rate is 10 times greater than the average value in the first 15–25 days after the eruption onset, and 5 times greater in the first 45 days, except for a not significant rate gap. In plot (b), the conditional rate is 10 times greater than average in the first 30 days, and 5 times greater in the first 45 days, with a few not significant gaps.

Figures 7c–7f consider the flank eruptions end and the earthquakes with (c) $I_x \geq$ V–VI and (d) $I_x \geq$ VII–VIII EMS. The conditional rate of earthquakes with $I_x \geq$ V–VI EMS is 5 times greater than the average value in the first 25–40 days after the eruption end. The rate of earthquakes with $I_x \geq$ VII–VIII EMS is 5 times greater than average in the first 30 days, with a short peak above 10 times. Figures 7e and 7f show that the peaks preceding
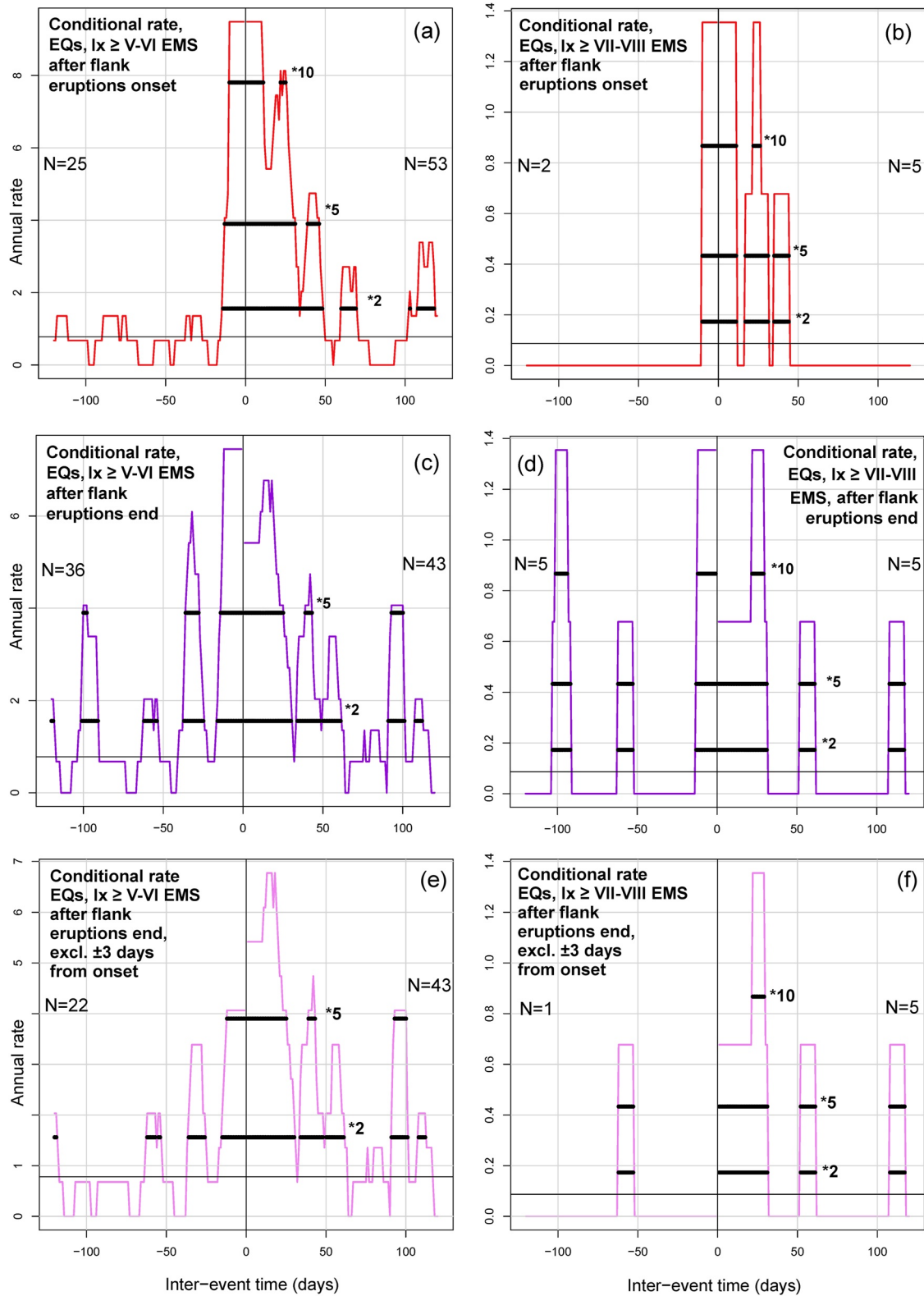
Figure 7. Conditional rates of earthquakes $<\pm 4$ months from flank eruptions. (a, c) The earthquakes with $I_x \geq$ V–VI EMS; (b, d) those with $I_x \geq$ VII–VIII EMS. (a, b) Consider the flank eruptions onset (red); (c–f) consider the flank eruptions end (purple and pink). (e, f) Exclude the earthquakes occurring in ± 2.5 days from the onset. A solid line marks the average annual rate of the earthquakes, and bold lines threshold rates 2, 5, and 10 times larger than the average value.

the eruption end are mostly related to a number of events almost contemporaneous with the eruption onset, thus it should be carefully evaluated, and not necessarily linked to the eruption end.

Note that in all cases the rates are also about 10 times greater than average in the last 10 days preceding the eruptions onset and end, 5 times if excluding the last day.

5. Spatial Statistical Analysis of Interevent Time Between Flank Eruptions and Earthquakes

In the following, we detail the spatial properties of the relationship between flank eruptions and major earthquakes in terms of geographical distribution of the eruptive fissures and systems of faults. This breaks the catalogs down into subsets, thus reducing the number of events considered but, nevertheless, enabling the description of significant differences in terms of probability of positive/negative interevent times, and conditional rates of the events. This analysis is not intended to describe stress direction obtained by focal mechanisms, which are not known for historical events, but aims at a simplified description of hazards correlation in a spatiotemporal framework. Note that the significance of rate gaps depends on the number of events, as pointed out in the previous section.

5.1. Spatial Analysis of the Eruptive Fissure Groups

The location and orientation of most of the historic eruptive fissures on Etna's flanks, together with the feeder-dykes of the previous activity, has been explained within the framework of a predominantly gravitational stress regime (McGuire & Pullen, 1989; McGuire et al., 1990, 1997). Nevertheless, flank instability interacts with the regional tectonic stress and the transient local stresses caused by inflation/deflation processes and dyke intrusion (Acocella & Neri, 2003; Azzaro et al., 2012a, 2013b; Bonforte et al., 2008, 2011). The stress regime that influences the propagation of eruptive fissures also affects the activation of a seismogenetic fault, and our analysis evaluates what type of statistical link exists between the two groups in different zones of the volcano.

In Figure 1, we show the post-1800 eruptive fissures considered in our analyses. We focus on the active portion of the fracture that erupted lava (e.g., Branca et al., 2017), discarding dry or not observed/buried fissures. This approach leads to treating all the eruptions consistently, avoiding questionable reconstructions and over-weighting of the recent events (much more documented). Therefore, we classify the flank eruptions in four spatial groups (i.e., systems) E1–E4 showing similar fissure orientations. In the case, an eruption opened fissures in multiple groups, we reported all of them separately, e.g., in the 2002–2003 event (see Figure 1; Andronico et al., 2005). Data Sets S1 and S3 in Supporting Information summarize these data; Azzaro and Neri (1992) further detail the eruptive fissures in 1971–1991. We note that, although the spatial groups E1–E4 are inspired by the volcano-tectonic sectors defined by Azzaro et al. (2012b), they have a descriptive purpose. In fact, other groups are possible, i.e., E1 and E2 could be characterized as a single group, E4 may not be a group, but simply diffusely distributed fissures that do not easily fit with the other groups. However, the description of these alternative cases can be easily deduced from the current analysis.

Figures 8a and 8b show the histograms of the groups, highlighting consistent distributions in the time spans 1600–2018 and 1800–2018 considered in the analysis. In particular, E1 is related to the South Rift and the southern wall of Valle del Bove, and includes 41–44% of the events; E2 is composed by the fissures in the northern wall of Valle del Bove, 25–28% of the events; E3 is the Northeastern Rift, 17–18% of the events, E4 the western flank, 13–14% of the events. After 1971, $16/21 = 76\%$ events affected sectors E1 and E2, while $6/21 = 29\%$ affected sectors E3 and E4 (the eruption of 2002–2003 is counted in both groups). These statistics are not significantly different from the spatial distribution, about 70% and 30%, respectively, observed in the last four centuries. Figure S15 in Supporting Information S1 reports the events of the spatial groups in the total event counting showing that in several cases short sequences of 3–5 eruptions were associated to the same spatial group.

The percentage of eruptions that is followed by a damaging earthquake depends on the spatial group considered. In particular, 30% of the eruption onsets in E1 are followed by an earthquake in 30 days, but only 12% of the eruptions in E2. Instead, 50% of the eruption onsets in E3 and E4 are followed by a damaging earthquake in 30–45 days. These percentage values are summarized in Table S8 in Supporting Information S1 and their
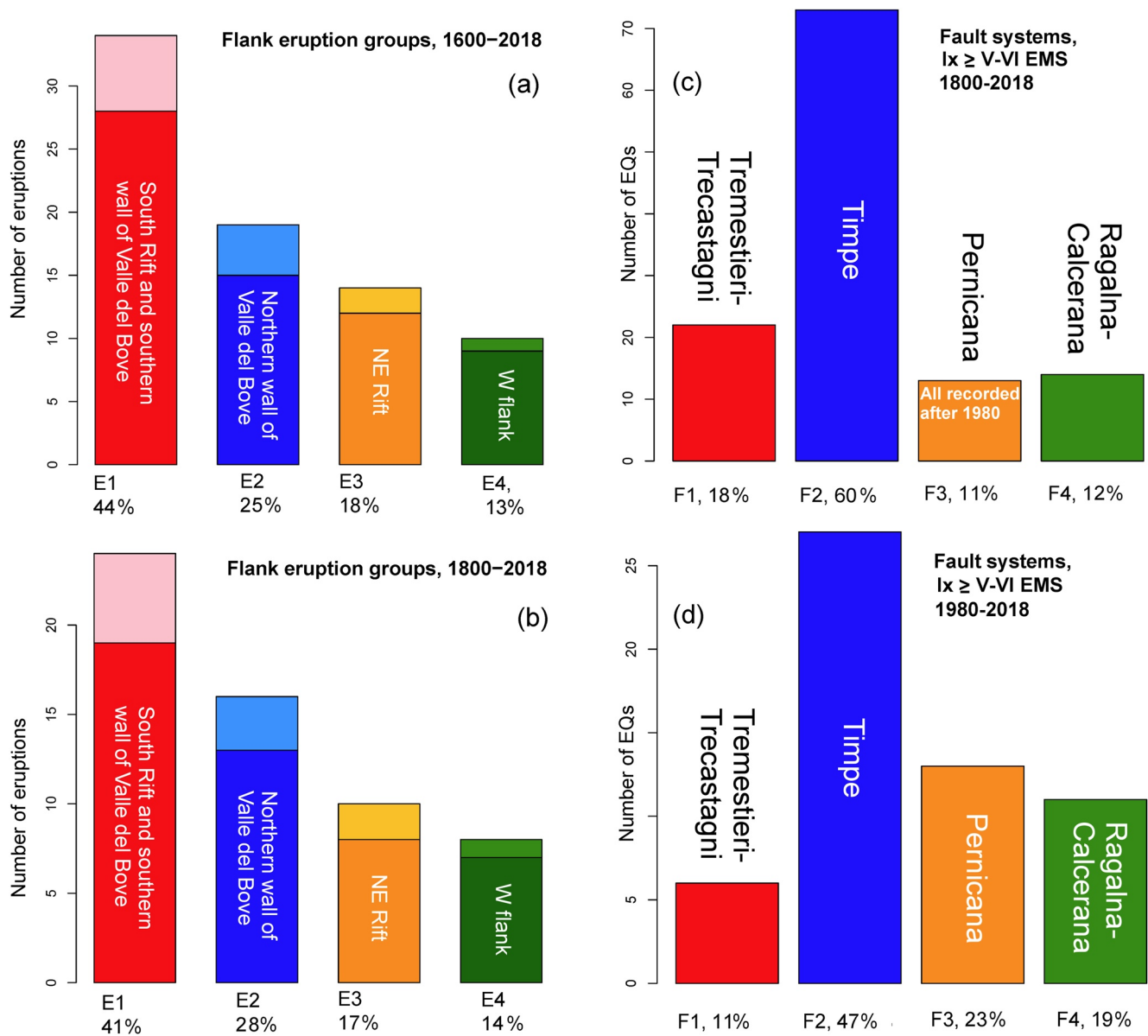
Figure 8. Histograms of eruptive fissures in the four spatial groups E1–E4 (a, b) and earthquakes with $I_x \geq$ V–VI EMS related to the four systems of seismogenic faults F1–F4 (c, d). The latter are mapped in Figure 1. Lighter colors mark the amount of "subterminal" eruptions in each group. Note that the data in (a, c) differ from (b) and (d), respectively, because of the time span considered. All the epicenters are mapped in Figure 2.

cumulative plot as a function of the interevent threshold is included in Figure S17 in Supporting Information S1. Additional estimates concerning only the earthquakes with $I_x \geq$ VII–VIII EMS are included in Figure S18 in Supporting Information S1.

As mentioned in Section 3.1, in the time span 1800–2018 some eruptions have uncertain classification as "subterminal" eruptions, i.e., above 2,850 m elevation, issued from fissures directly propagating from the summit craters. They are equally distributed in all groups, and represent about 20% of the fissures. However, they give a negligible contribution in terms of interevent times with respect to the major earthquakes, as reported in Data Set S7 in Supporting Information S1. Therefore, if we excluded all the flank eruptions occurred above 2,850 m a.s.l. from the analysis, the percentage of eruptions that is followed by a damaging earthquake would increase by a multiplicative factor equal to 1.15–1.20.

Figure 9 reports the conditional rates of earthquakes, $I_x \geq$ V–VI EMS, in ±4 months from flank eruptions in the spatial groups E1, E2, and E3. As in Figure 6, pie charts evaluate the percentages of positive and negative inter-event times. All measured values are reported in Table S9 in Supporting Information S1. Figure 9 also displays the total number N of earthquakes observed before and after the eruptions onset/end.

In Figure 9a, the conditional rate following a flank eruption onset in E1 is consistent with the analysis in Section 4. In Figure 9b, albeit only 12% of the eruption onsets in E2 are followed by damaging earthquakes, their conditional rate still increases significantly after such an event, due to the likely occurrence of multiple earthquakes. In particular, an eruption onset in E2 is followed by an apparent rate gap of 15 days. Although visually evident, this delay is too short to be statistically relevant according to Equation 8. Then the rate is 10 times greater than the average value up to 45 days and 5 times greater up to 70 days, except for a few other not significant rate gaps. In Figure 9c, the conditional rate following a flank eruption onset in E3 is 20 times greater than the average value in the first 15 days, 10 times in the first 45 days, 5 times in the first 65 days, evidencing a stronger and longer-lasting correlation than in the overall case.

Figures 9b, 9d, and 9f show that the earthquake rate increases also after the eruption end. As in Figure 6, we excluded the earthquakes preceding the eruption if they occurred <2.5 days from the eruption onset. In all cases, the earthquake rates following eruption ends in E1, E2, or E3 are similar to the estimates following eruption onset.

Figure S20 in Supporting Information S1 reports the analysis in the spatial group E4, which are similar to the global data set, but among the earthquakes in ±4 months, about 90% follow the eruption onset instead of 67%.

5.2. Spatial Analysis of the Fault Systems

The reconstruction of the seismic histories of the faults enabled us to break down the damaging earthquakes in the CMTE catalog into subsets of data based on the association of earthquakes and causative faults (Azzaro, 1999; Azzaro et al., 2017).

According to the seismotectonic model (Azzaro et al., 2012b, 2013b), we considered the four systems of faults mapped in Figure 2. The Timpe system (F2) and the Pernicana fault (F3) are the most active tectonic features of Mt. Etna, dissecting the entire eastern flank and intersecting the volcano-tectonic structures of the NE Rift and Valle del Bove depression. In addition, we have considered the Tremestieri-Trecastagni faults (F1) in the southern flank, and the Ragalna-Calcerana fault systems (F4), in the southwestern flank.

The seismogenic potential of all these faults is significant for the urbanized areas of Etna, particularly for the eastern sector of the volcano (Azzaro et al., 2013a, 2016). Among these, the Timpe system in particular (F2), is responsible for the most damaging earthquakes that reach epicentral intensities I_x up to degree IX-X EMS, which occur individually or as seismic swarms, with recurrence times of ca. 70 years for the largest events. While the F2 and F4 fault systems are characterized by less frequent and moderate earthquakes, the Pernicana fault system (F3) is a complex structure playing a crucial role in the dynamics of the volcano (Azzaro et al., 2013b; Bonforte et al., 2007; Neri et al., 2004). Unfortunately, its seismic history is documented only for the last decades because the area crossed by the fault has been urbanized since the late 1970s (Azzaro, 1997; Azzaro et al., 1998a, 1998b). However, its seismotectonic behavior is well constrained and several studies have recognized that this fault zone localized earthquakes in connection with the eruptive activity (Acocella et al., 2003; Bonaccorso et al., 2013, 2017; Bonaccorso & Giampiccolo, 2020; Currenti et al., 2012; Ruch et al., 2013).

Figures 8c and 8d show the histograms of the four groups with $I_x \geq$ V–VI EMS, either (a) in 1800–2018, 122 events, or (c) in 1980–2018, 57 events. In particular, in 1800–2018, 18% of the earthquakes with $I_x \geq$ V–VI EMS belong to F1, 60% to F2, 11% to F3, 12% to F4. In contrast, 88% of the 17 earthquakes with $I_x \geq$ VII–VIII EMS related to F2 fault system, one event to F3, one event to F4, none to F1. Therefore, this subrecord is essentially concentrated in the Timpe fault system (F2). Note that in 1980–2018, 10% of the earthquakes with $I_x \geq$ V–VI EMS are related to F1, 47% to F2, 23% to F3, 19% to F4, as a consequence of the historical under-recording of the earthquakes occurring in the less urbanized sectors F3 and F4.

Figure S16 in Supporting Information S1 marks the various fault systems in the total earthquake counting; all the local subrecords show evidence of spatiotemporal clustering.
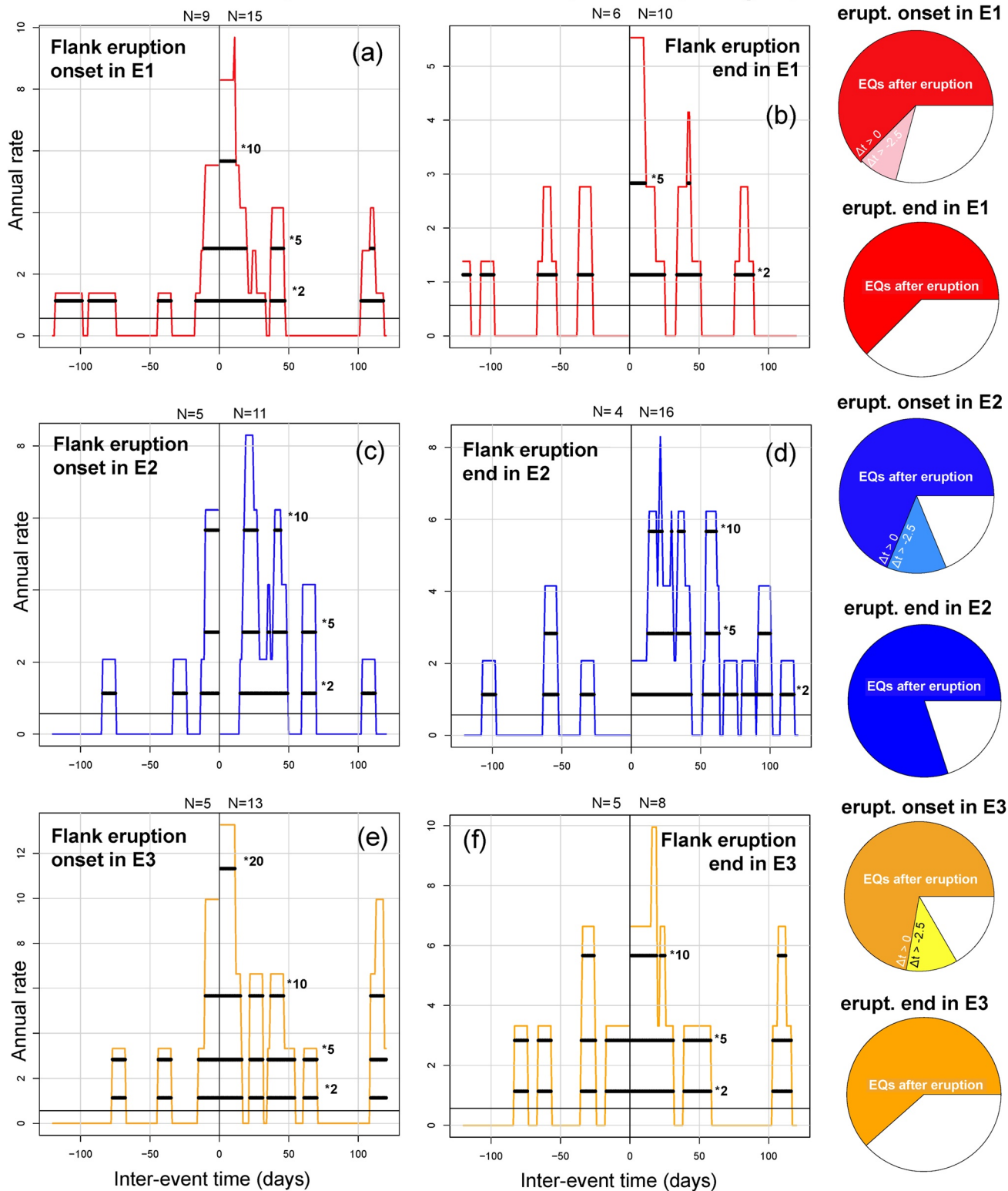
Figure 9.

We first estimated the percentage of earthquakes of each fault system that followed a flank eruption. In particular, 27% of the damaging earthquakes in F1 followed an eruption onset in 45 days, 23% of the earthquakes in F2, 8% in F3, 21% in F4. These percentage values are summarized in Table S8 in Supporting Information S1, and their cumulative plot as a function of the interevent threshold is included in Figure S19 in Supporting Information S1.

Figure 10 reports the conditional rates of earthquakes, $I_x \geq$ V–VI EMS, related to the systems of faults F1, F2, and F3, $< \pm 4$ months from flank eruptions. The rate of F3 is calculated after 1980. Pie charts evaluate the percentages of positive and negative-valued interevent times, all reported in Table S9 in Supporting Information S1. The figure also displays the total number N of events observed before and after the eruption onset/end.

In Figures 10a and 10c, the conditional rate in F1 and F2 is similar to the global data set, but, among the earthquakes in ± 4 months, about 90% follow the eruption onset instead of 67%. In system F1, following a flank eruption onset we observe a peak 20 times higher than average rate at 35–45 days from the eruption. This delayed peak, despite being visually evident, is not statistically significant according to Equation 8. In Figure 10e, the conditional rate in F3 preceding a flank eruption onset is 20 times greater than the average value in the last 15 days before it. Therefore, system F3 shows an opposite behavior compared to the other systems, and the earthquakes tend to precede the eruption onsets rather than following them.

Figures 10b, 10d, and 10f show the conditional earthquake rate with respect to the eruption end. Similar to the global case, some of the peaks preceding the eruption are closely related to the eruption onset and are excluded from the analysis. In Figures 10b and 10d, the conditional rates in F1 and F2 following a flank eruption end are similar to the estimates following eruption onset. In Figure 10f, the conditional rate in F3 preceding a flank eruption end is only based on one event, hence not statistically significant and consistent with the average rate.

Figure S20 in Supporting Information S1 reports the analysis in the F4 system, which still shows an increase of earthquake rate, but symmetrically distributed with respect to the eruption onset or end.

5.3. The Pernicana Fault Case Study

We detailed the analysis of the Pernicana fault (F3) since we found that major earthquakes in F3 are more likely to precede flank eruptions rather than to follow. The CMTE subdata set of F3 includes 37 earthquakes, all occurring after 1980, of which 13 had $I_x \geq$ V–VI and one had $I_x \geq$ VII–VIII EMS, in 2002.

We observe that 30% of the earthquakes in F3 precede a flank eruption onset. In addition, 40% of the earthquakes in F3 are followed by an $I_x \geq$ V–VI EMS earthquake in another system of faults within 45 days, 14% of them by an $I_x \geq$ VII–VIII EMS earthquake. These percentage values are summarized in Table S8 in Supporting Information S1, and their cumulative plot as a function of the interevent threshold is included in Figure S21 in Supporting Information S1.

Figure 11 shows the conditional rates of major earthquakes related to the systems of faults F1, F2, and F4 $< \pm 4$ months from any earthquake in F3. We also show the pie charts of positive and negative values, and display the number N of events observed before and after the eruption onset/end. All measured values are reported in Table S9 in Supporting Information S1.

Figures 11a and 11c consider the earthquakes with $I_x \geq$ V–VI EMS, the conditional rate following an event in F3 is 10 times greater than the average value in the first 70 days, except for not significant rate gaps. There are peaks above 20-times average at 20–45 days. Figures 11b and 11d consider the earthquakes with $I_x \geq$ VII–VIII EMS; in this case, the conditional rate following an event in F3 is 40 times greater than the average value in the first 15 days. Several other peaks of 10-times average rate both precede and follow it, denoting a small but unusual number of major earthquakes with $I_x \geq$ VII–VIII EMS in ± 50 days from an event in F3, and decreasing slowly. These results confirm the complex role of the Pernicana fault in the geodynamic and volcanic processes at Mt. Etna.

Figure 9. Conditional rates of earthquakes, $I_x \geq$ V–VI EMS, $< \pm 4$ months from flank eruptions in spatial groups (a, b) E1, (c, d) E2, (e, f) E3. Pie charts of the positive values (dark colors), negative values in [−2.5, 0] days (light colors), and lower than −2.5 days (white) are reported. (a, c, e) Consider the flank eruptions onset; (b, d, e) consider the flank eruptions end, excluding the earthquakes occurring in ± 2.5 days from the onset. Results without excluding these earthquakes are in Data Set S6 in Supporting Information S1. Related histograms of interevent times are in Data Set S7 in Supporting Information S1. All values in the pie charts are in Table S9 in Supporting Information S1. A solid line marks the average annual rate of the earthquakes, and bold lines threshold rates 2, 5, 10, and 20 times larger than the average value. Figure S20 in Supporting Information S1 reports the analysis in the spatial group E4.
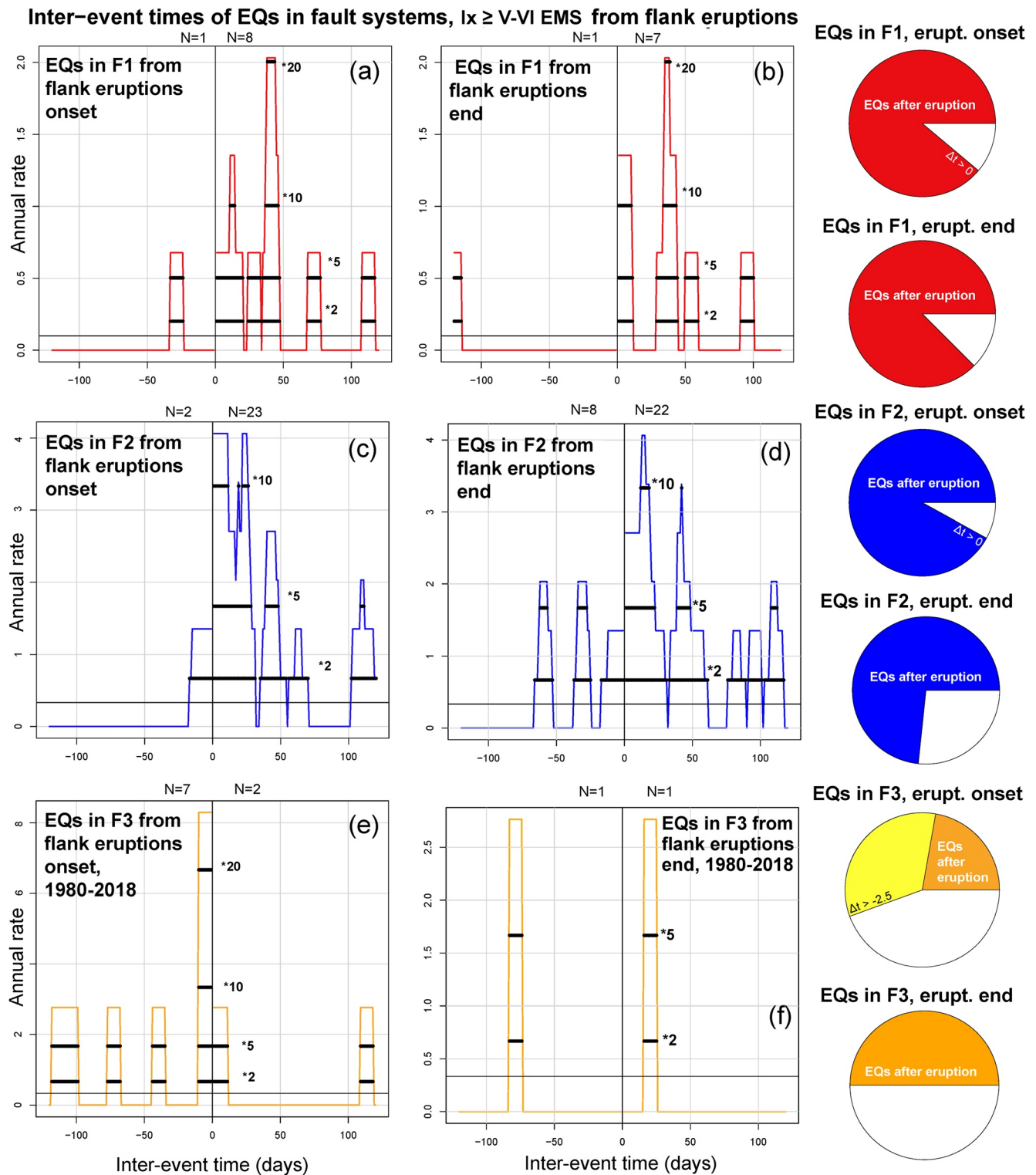
Figure 10. Conditional rates of earthquakes, $I_x \geq$ V–VI EMS, related to the systems of faults (a, b) F1, (c, d) F2, (e, f) F3 after 1980, $< \pm 4$ months from flank eruptions. Pie charts of the positive values (dark colors), negative values in [−2.5, 0] days (light colors), and lower than −2.5 days (white) are reported. (a, c, e) Consider the flank eruptions onset; (b, d, e) consider the flank eruptions end, excluding the earthquakes occurring in ±2.5 days from the onset. Results without excluding these earthquakes are in Data Set S6 in Supporting Information S1. Related histograms of interevent times are in Data Set S7 Supporting Information S1. All values in the pie charts are in Table S9 in Supporting Information S1. A solid line marks the average annual rate of the earthquakes, and bold lines threshold rates 2, 5, 10, and 20 times larger than the average value. Figure S20 in Supporting Information S1 reports the analysis in the system of faults F4.
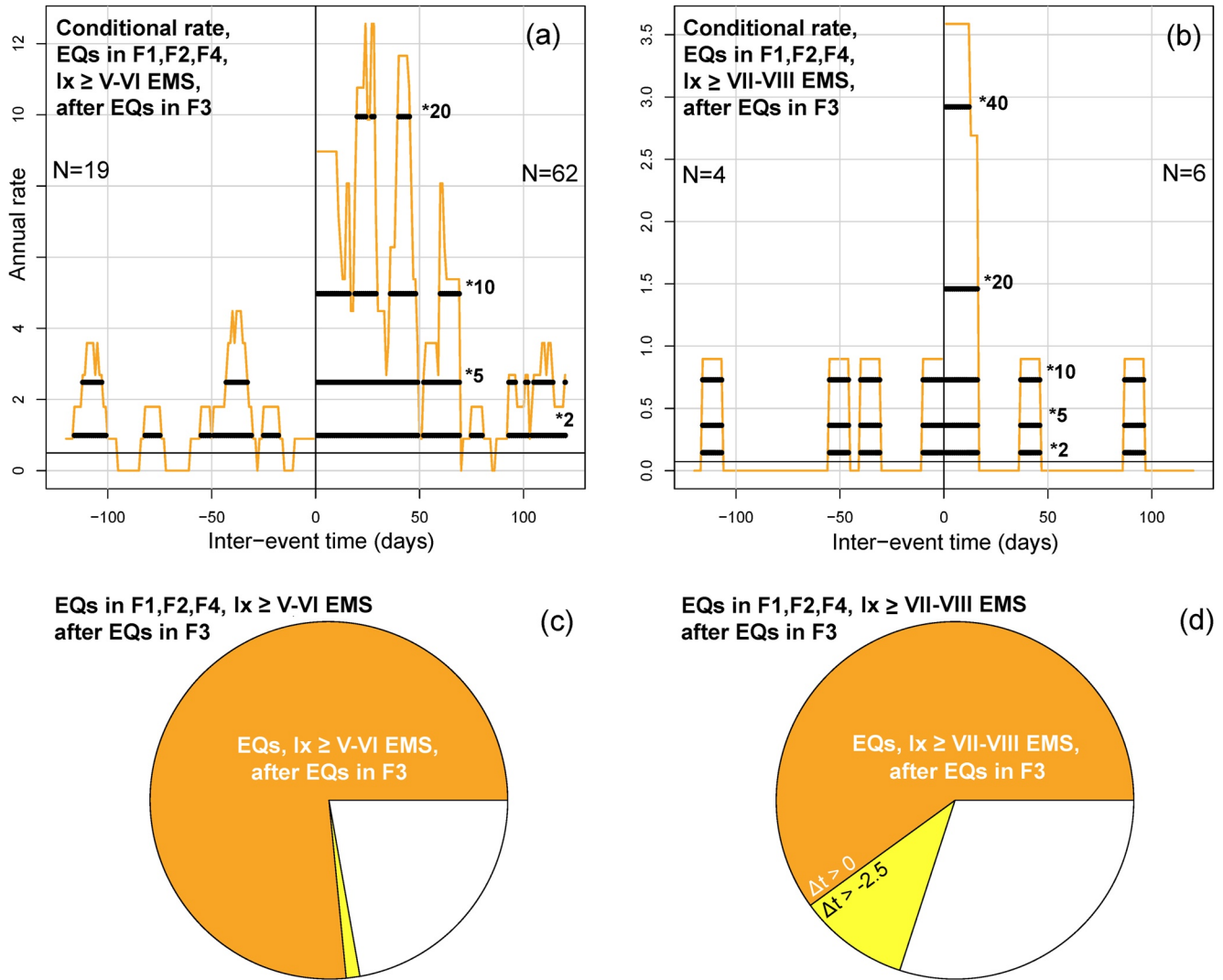
Figure 11. Conditional rates of major earthquakes related to the systems of faults F1, F2, and F3, < ±4 months from any earthquake related to F3. Pie charts of the positive values (orange), negative values in [−2.5, 0] days (yellow), and lower than −2.5 days (white) are reported. Related histograms of interevent times are in Data Set S7 in Supporting Information S1. All values in the pie charts are in Table S9 in Supporting Information S1. A solid line marks the average annual rate of the earthquakes, and bold lines threshold rates 2, 5, 10, 20, and 40 times larger than the average value. (a, c) Considers the major earthquakes with $I_x \geq$ V–VI EMS; (b, d) those with $I_x \geq$ VII–VIII EMS. Similar results only considering the earthquakes in F3 with $I_x \geq$ V–VI EMS are in Figure S22 in Supporting Information S1.

6. Results Interpretations and Limitations

In the following, we refer to the meaning and contextualization of our statistical methods, as well as the main sources of uncertainty deriving from input data and how they affect our results; finally, we also discuss the consistence with physical interpretations of the results, and possible comparison with other volcanic systems.

6.1. Statistical Methods Applied and Their Contextualization

The most significant element of our analysis is the data set of interevent time between the time series under investigation. We studied this data set of time differences both in terms of skewness with respect to the null time (e.g., Figure 6), and in terms of the conditional rates described by it (e.g., Figure 7). This approach requires selecting a time limit, in our case ±4 months, i.e., the upper and lower bounds of the interevent times that are considered.

This time limit is not an a-priori assumption on the duration of the described correlation, which in fact is shorter than that.

Our definition of the conditional rates by using a windowed time-lag approach is the key idea behind the formulation of the classical tests in Cox (1955) and Brillinger (1976), already applied to outdated Etna historical records by Sharp et al. (1981), Nercessian et al. (1991), and Mulargia (1992). In any case, the conditional rates and their cumulative functions, while adopted in these tests, were never presented or discussed directly, neither globally or locally in space. Our approach is similar to a kernel smoothing that employs a step function (Bevilacqua et al., 2018); however, given the relative low population of data, optimally determining the bandwidth would have led to an excessive smoothing of the result, hiding the sharp changes in the rate that potentially occur when a correlated phenomenon takes place. Thus, we preferred to fix a relative short lag, i.e., 10 days, and then set up a statistical testing for the statistical significance of the observed rate gaps.

An interesting result of our study is the revised modeling of both past eruption and earthquake records, in terms of a "slowly varying" Poisson process. They are nonhomogeneous Poisson processes (e.g., Daley & Vere Jones, 2005) in which the time-dependent intensity function is obtained by decomposing the entire time interval considered in 25-year long subintervals, and imposing a constant average rate over these subsets. This simple approach, also followed by Sharp et al. (1981), enables the application of the Cox (1955) test to time series that are not homogeneous in time. The Poissonian nature of the flank eruption series is still consistent with previous analyses of temporal nonstationarity, because a "slowly varying" rate allows for change points in the eruptive frequency (Bebbington, 2007; Mulargia et al., 1987; Smethurst et al., 2009).

Finally, we note that the spatial classification adopted for eruptive fissures and seismogenic faults appears rather simple, but it is strictly based on the volcano-tectonic characteristics of Etna (see Azzaro et al., 2012b and references therein). We took this approach for several reasons. First, our approach is significantly robust—very few events could be considered uncertainly assigned; we tested the sensitivity of switching their assignment, and it is negligible. Second, precise mapping of the total extent of the eruptive fissures is not possible for older historical events; reaching a time-homogeneous spatial detail is not possible either. Third, with four groups of eruptive/seismotectonic systems, the number of considered events is still sufficient to enable statistically significant observations, but increasing spatial classes or setting up a spatially continuous model would create issues of statistical significance. A similar discrete spatial classification was followed for the Campi Flegrei area (Neapolitan volcanic district) and tested against other methods in Bevilacqua et al. (2015, 2016).

6.2. Main Sources of Uncertainty and Data Limitations

We considered the flank eruptions in terms of onset and end of the eruptive activity. Although we studied these two time series separately, we filtered out the earthquakes possibly related to the eruption onsets while analyzing the eruption ends. In fact, when an eruption is not characterized by a long duration, the possible correlation of the earthquakes with the onset or the end of the eruptive activity is hardly distinguishable. Nevertheless, the duration of the eruption is additional information that might be considered in the analysis—e.g., to test if some earthquakes occurred during the eruption or not. However, we focused on the onset and the end of the eruptions because they have a precise temporal determination that allows calculating the interevent time with respect to the earthquakes. Moreover, the state of the volcano during the onset and, secondarily, the end of an eruption, is characterized by significant ground deformations of the volcanic edifice (Bonaccorso & Giampiccolo, 2020; Bonaccorso et al., 2013; Bonforte et al., 2011), inducing stress changes that may act on the seismogenic faults near rupture conditions.

Summit eruptions may also precede, days to weeks before (or even months), the onset of flank eruptions, and strong earthquakes. However, these phenomena are very difficult to evaluate from historical records, since data are not homogeneous and largely incomplete, appearing questionable whether the different types of persistent summit activity (strombolian, ash emissions, lava fountains), with different duration and intensity, might have the same significance at all times. Therefore, from our analysis and data we cannot conclusively claim that summit eruptions are or are not correlated with increased seismic hazard.

Another limitation is related to the possibility that a dyke intrusion not followed by a flank eruption might trigger earthquakes, or that a small-sized flank eruption is buried and not adequately addressed in the catalog. We cannot exclude that some of the earthquakes apparently unrelated to eruptions have indeed occurred as a consequence of

an aborted magma intrusion. Similarly, the seismic history of Pernicana fault and, secondarily, that of the western fault system, are well documented only for the last few decades, because of the relatively recent urbanization of those regions. That is, we do not know how many historical eruptions before 1980 occurred temporally close to an unrecorded seismic event. Given these limitations, the spatial analysis presented in Section 5.2 studied the different systems of faults also in terms of the differing lengths of their seismic histories.

6.3. Physical Models of Earthquakes-Eruptions Interactions

This study has some similarities with the research on the conjecture that, a large earthquake can trigger subsequent volcanic eruptions, sometimes over long distance and time scales (Hill et al., 2002; Nishimura, 2017; Sawi & Manga, 2018). Several mechanisms have been proposed to explain triggering through changes in magma overpressure or through failure of rocks surrounding stored magma (Manga & Brodsky, 2006). This may involve large-scale seismic resonance mechanisms (Namiki et al., 2019).

For example, the 1707 M_w 8.7 Hoei earthquake preceded by 49 days the largest historical eruption of Mt. Fuji (Chesley et al., 2012). The 1992 Landers earthquake in California triggered seismicity in the Long Valley caldera region which also experienced a significant coincident deformation transient (Linde & Sacks, 1998). In 2012, three $M_w \geq 7.3$ earthquakes struck Central America within a period of 10 weeks; subsequently, some volcanoes in the region erupted a few days after, while others took months or even years to erupt (Gonzàlez et al., 2021). Several other examples can be found in literature (Bell et al., 2021; Cannata et al., 2010; Farías & Basualto, 2020; Walter, 2007).

In summary, although most types of volcanoes may be seismically triggered, though require specific combinations of volcanic and seismic conditions—triggering is unlikely unless the system is "primed" for eruption (Seropian et al., 2021). Further statistical analysis supported this supposition, indicating that seismicity most likely initiates an already looming eruption (Bebbington & Marzocchi, 2011). In fact, once a magmatic system reaches a critical state, the timing of the eruption can be modulated by external factors. Whether such mechanisms actually trigger an eruption depends on both the magma conditions and the characteristics of the external force (Caricchi et al., 2021).

However, in this study, we mostly observed the opposite phenomenon, i.e., an increased probability of major earthquakes after the occurrence of volcanic eruptions. This is less studied in literature, but also observed in a global perspective. The analysis of Global Volcanism Program catalog and the global earthquake catalog of Columbia University, available since 1976, showed that M_w 5–6 earthquakes can be activated within a horizontal distance of 50 km from volcanoes for about 0.3 years after the initiation of an eruption. About 13% of volcanic eruptions are accompanied by these earthquakes. Their probability of occurrence is about 5 times larger than normal for 0.3 years after an eruption (Nishimura, 2018). This latter finding is consistent with our results for Etna, although we considered smaller magnitudes and closer distances, and we estimated a shorter duration of the probability increase, i.e., 70 days at most.

Similar to the case of "triggered" volcanism described above, the explanation of "triggered" earthquakes is challenging. However, the stress changes induced by dyke intrusion has the potential to anticipate rupture in faults already prone to slip, i.e., loaded by significant pre-existing stresses. Moreover, dyke intrusions and the opening of eruptive fissures may speed-up gravity-driven large-scale movements that subsequently cause strong earthquakes. This second mechanism could explain some of the longest observed delays in our case study, rather than an immediate viscoplastic response.

The Kilauea eruption of 2018 probably shared similar mechanisms: the backup in the magma plumbing system at the long-lived Puʻu ʻŌʻō eruption site caused widespread pressurization in the volcano, driving magma into the lower flank; magma reached the surface on 3 May, marking the onset of the eruption; the next day, an M_w 6.9 earthquake occurred on Kīlauea's south flank—the largest earthquake in Hawaiʻi in 43 years (Patrick et al., 2020). The analysis of seismological and geodetic data sets showed the creep on the décollement constantly altered the stress accumulation, while dyke intrusion triggered the occurrence of the large earthquake (Chen et al., 2019).

Table 1
Summary of the Conditional Daily Average Rates and Total Probabilities

		Average daily rate (%)	Relative increment	Total probability (%)
(a) Flank eruptions onset		0.06	—	—
1–10 days after:	EQs with $I_x \geq 5$–6 EMS	0.37	6	4
1–45 days after:	EQs in F3 (Pernicana)	0.24	4	11
(b) Earthquakes with $I_x \geq 5$–6 EMS		0.21	—	—
1–45 days after:	Flank eruptions onset (f.e.o.)	1.6	8	32
	f.e.o. in E1 (South Rift)	1.1	5	30
	f.e.o. in E2 (North of VdB)	1.1	5	12
	f.e.o. in E3 (NE Rift)	2.0	10	50
	f.e.o. in E4 (West flank)	1.4	7	50
	Flank eruptions end	1.1	5	25
	EQs in F3 (Pernicana)	2.2	10	34
(c) Earthquakes with $I_x \geq 7$–8 EMS		0.02	—	—
1–45 days after:	Flank eruptions onset (f.e.o.)	0.22	11	10
	f.e.o. in E1 (South Rift)	0.27	14	13
	f.e.o. in E2 (North of VdB)	0.14	7	7
	f.e.o. in E3 (NE Rift)	0.65	33	30
	f.e.o. in E4 (West flank)	0.27	14	13
	Flank eruptions end	0.13	7	7
	EQs in F3 (Pernicana)	0.29	15	14

Note. (a) Flank eruptions and (b, c) major earthquakes 1 to 10 or 45 days from statistically significant other phenomena, and their comparison with the unconditional average rates of the same phenomena. The total probabilities are not the product of the average rate and the number of days considered, because of the chance of multiple events occurring. Some probabilities may take greater values if we assumed a few weeks' longer periods. The average rates are obtained from Figures 2, 3, 7, 9, and 11, and the total probabilities from Table S8 in Supporting Information S1.

7. Conclusions

We investigated the long-term, centennial behavior of Etna by testing the statistical relationships between flank eruptions and major earthquakes, a topic tackled in several studies of 1980–90s. Our efforts were threefold. First, we revisited the main results of previous works and improve the significance of the statistical correlation in an up-to-date framework of knowledge deriving from recent multidisciplinary studies. This was achieved by applying the key ideas of the test of Cox (1955) to the most recent releases of the historical catalogs. Second, we produced a quantitative evaluation of how much, how long, and where the effusive eruptions and major earthquakes are statistically linked, key information to jointly deal with the two main components of hazard at Etna. Third, we interpreted these results in terms of plausible geophysical motivations and international case studies.

In detail, we focused on the estimation of the average rates of earthquakes occurring in the first months after a flank eruption, which is the combination of two factors: (a) the probability that an eruption is followed by an earthquake, (b) the probability that multiple damaging earthquakes occur after the same eruption. Table 1 summarizes the conditional daily average rates of flank eruption and major earthquakes 1 to 10 or 45 days from statistically significant other phenomena, their comparison with the long-term (i.e., unconditional) average rates of the same phenomena, and the total probabilities of occurrence in the considered interval. More specific results of this study are summarized in Text S25 in Supporting Information S1.

The main points emerging from this analysis are:

1. The sequence of flank eruptions occurring since 1600 are statistically compatible with Poisson processes with "slowly varying" rate, i.e., equal to a 25-year average.

2. It is statistically evident that major earthquakes at Etna are not independent from the flank eruptions, either considering onset or end. 30% of flank eruption onsets precede a major earthquake (i.e., $I_x \geq$ V–VI EMS) of 30 days or less; 18% of damaging earthquakes follow a flank eruption onset within 30 days or less. These probabilities are about 35% and 20% if we exclude all the flank eruptions occurring above 2,850 m a.s.l. from the analysis.

3. The probability of major earthquakes increases of 5–10 times after the onset and the end of flank eruptions; this effect lasts for 30–45 days; a similar increment occurs in the 10 days preceding the onset and the end, mainly concentrated in the last day.

4. Although only 12% of the eruptions in the northern wall of Valle del Bove precede a major earthquake, the conditional rate is still 5 times greater than the average up to 70 days, due to the likely occurrence of multiple earthquakes.

5. Fifty percentage of the eruptions on the northeastern flank precede a major earthquake; they produce a longer and more significant rate increase of earthquakes, also after their end, than the one estimated for the other flanks—up to 10–20 times and for 65–70 days.

6. Thirty percentage of the earthquakes along the Pernicana fault precede a flank eruption and 40% of them precede a major earthquake in other fault systems; they increase by 10–20 times the rate of both phenomena, and this effect lasts for 45–70 days.

Our results, based on observational historical data, are not aimed at proposing new physical models of behavior of the volcano. They can be discussed and explained in terms of the existing physical interpretations, constrained by the instrumental monitoring of the most recent eruptions. Nevertheless, they may represent the quantitative basis for a multihazard assessment to improve the emergency planning and help decision makers to face future eruptive crises at Mt. Etna.

Data Availability Statement

The historical catalog of the Etnean earthquakes from 1633 to 2018 is available in Azzaro and D'Amico (2019). The historical catalog of flank eruptions of Etna from 1682 to 2002 is available in Branca and Del Carlo (2005). All the Data Sets S1–S7, updated and analyzed or generated during the current study, are available in the repository https://doi.org/10.5281/zenodo.6855359.

References

Acocella, V., Behncke, B., Neri, M., & D'Amico, S. (2003). Link between major flank slip and eruptions at Mt. Etna (Italy). *Geophysical Research Letters*, *30*(24), 2286. https://doi.org/10.1029/2003GL018642

Acocella, V., & Neri, M. (2003). What makes flank eruptions? The 2001 Etna eruption and the possible triggering mechanisms. *Bulletin of Volcanology*, *65*, 517–529. https://doi.org/10.1007/s00445-003-0280-3

Alparone, S., Barberi, G., Cocina, O., Giampiccolo, E., Musumeci, C., & Patanè, D. (2012). Intrusive mechanism of the 2008–2009 Mt. Etna eruption: Constraints by tomographic images and stress tensor analysis. *Journal of Volcanology and Geothermal Research*, *229–230*, 50–63. https://doi.org/10.1016/j.jvolgeores.2012.04.001

Andronico, D., Branca, S., Calvari, S., Burton, M., Caltabiano, T., Corsaro, R. A., et al. (2005). A multi-disciplinary study of the 2002-03 Etna eruption: Insights into a complex plumbing system. *Bulletin of Volcanology*, *67*, 314–330. https://doi.org/10.1007/s00445-004-0372-8

Andronico, D., & Lodato, L. (2005). Effusive activity at Mount Etna volcano (Italy) during the 20th century: A contribution to volcanic hazard assessment. *Natural Hazards*, *36*, 407–443. https://doi.org/10.1007/s11069-005-1938-2

Azzaro, R. (1997). Seismicity and active tectonics along the Pernicana fault, Mt. Etna (Italy). *Acta Vulcanologica*, *9*(1/2), 7–14.

Azzaro, R. (1999). Earthquake surface faulting at Mount Etna volcano (Sicily) and implications for active tectonics. *Journal of Geodynamics*, *28*, 193–213. https://doi.org/10.1016/s0264-3707(98)00037-4

Azzaro, R., & Barbano, M. S. (1996). Relationship between seismicity and eruptive activity at Mt. Etna volcano (Italy) as inferred from historical record analysis: The 1883 and 1971 case histories. *Annali di Geofisica*, *39*(2), 445–461.

Azzaro, R., Barbano, M. S., Antichi, B., & Rigano, R. (2000). Catalogo Macrosismico dei Terremoti Etnei dal 1832 al 1998. *Acta Vulcanologica*, *12*, 3–36.

Azzaro, R., Barbano, M. S., D'Amico, S., & Tuvè, T. (2006). The attenuation of seismic intensity in the Etna region and comparison with other Italian volcanic districts. *Annals of Geophysics*, *49*(4/5), 1003–1020.

Azzaro, R., Barbano, M. S., D'Amico, S., Tuvè, T., Albarello, D., & D'Amico, V. (2008). First studies of probabilistic seismic hazard assessment in the volcanic region of Mt. Etna (Southern Italy) by means of macroseismic intensities. *Bollettino di Geofisica Teorica e Applicata*, *49*(1), 77–91.

Azzaro, R., Barbano, M. S., Rigano, R., & Vinciguerra, S. (2001). Time seismicity patterns affecting local and regional fault systems in the Etna region: Preliminary results for the period 1874-1913. *Journal of the Geological Society*, *158*, 561–572. https://doi.org/10.1144/jgs.158.3.561

Azzaro, R., Barberi, G., D'Amico, S., Pace, B., Peruzza, L., & Tuvè, T. (2017). When probabilistic seismic hazard climbs volcanoes: The Mt. Etna case, Italy—Part 1: Model components for sources parameterization. *Natural Hazards Earth System Science*, *17*, 1981–1998. https://doi.org/10.5194/nhess-17-1981-2017

Azzaro, R., Bonforte, A., Branca, S., & Guglielmino, F. (2013a). Geometry and kinematics of the fault systems controlling the unstable flank of Etna volcano (Sicily). *Journal of Volcanology and Geothermal Research*, *251*, 5–15. https://doi.org/10.1016/j.jvolgeores.2012.10.001

Azzaro, R., Bonforte, A., D'Amico, S., Guglielmino, F., & Scarfì, L. (2020). Stick-slip vs. stable sliding fault behaviour: A case-study using a multidisciplinary approach in the volcanic region of Mt. Etna (Italy). *Tectonophysics*, *790*, 228554. https://doi.org/10.1016/j.tecto.2020.228554

Azzaro, R., Branca, S., Giammanco, S., Gurrieri, S., Rasà, R., & Valenza, M. (1998a). New evidence for the form and extent of the Pernicana fault system (Mt. Etna) from structural and soil-gas surveying. *Journal of Volcanology and Geothermal Research*, *84*, 143–152. https://doi.org/10.1016/s0377-0273(98)00036-5

Azzaro, R., Branca, S., Gwinner, K., & Coltelli, M. (2012a). The volcanotectonic map of Etna volcano, 1:100.000 scale: An integrated approach based on a morphotectonic analysis from high-resolution DEM constrained by geologic, active faulting and seismotectonic data. *Italian Journal of Geosciences*, *131*, 153–170. https://doi.org/10.3301/ijg.2011.29

Azzaro, R., & Castelli, V. (2015). Materiali per un catalogo di terremoti etnei dal 1600 al 1831. *Quaderni di Geofisica*, *123*, 1–284.

Azzaro, R., & D'Amico, S. (2019). *Catalogo Macrosismico dei Terremoti Etnei (CMTE)*. Ufficio Dati, Istituto Nazionale di Geofisica e Vulcanologia. https://doi.org/10.13127/cmte

Azzaro, R., D'Amico, S., Peruzza, L., & Tuvè, T. (2012b). Earthquakes and faults at Mt. Etna (southern Italy): Problems and perspectives for a time-dependent probabilistic seismic hazard assessment in a volcanic region. *Bollettino di Geofisica Teorica e Applicata*, *53*, 75–88.

Azzaro, R., D'Amico, S., Peruzza, L., & Tuvè, T. (2013b). Probabilistic seismic hazard at Mt. Etna (Italy): The contribution of local fault activity in mid-term assessment. *Journal of Volcanology and Geothermal Research*, *251*, 158–169. https://doi.org/10.1016/j.jvolgeores.2012.06.005

Azzaro, R., D'Amico, S., & Tuvè, T. (2011). Estimating the magnitude of historical earthquakes from macroseismic intensity data: New relationships for the volcanic region of Mount Etna (Italy). *Seismological Research Letters*, *82*, 533–544. https://doi.org/10.1785/gssrl.82.4.533

Azzaro, R., D'Amico, S., & Tuvè, T. (2016). Seismic hazard assessment in the volcanic region of Mt. Etna (Italy): A probabilistic approach based on macroseismic data applied to volcano-tectonic seismicity. *Bulletin of Earthquake Engineering*, *17*, 1813–1825. https://doi.org/10.1007/s10518-015-9806-2

Azzaro, R., Ferreli, L., Michetti, A. L., Serva, L., & Vittori, E. (1998b). Environmental hazard of capable faults: The case of the Pernicana fault (Mt. Etna, Sicily). *Natural Hazards*, *17*(2), 147–162. https://doi.org/10.1023/a:1008034422086

Azzaro, R., & Neri, M. (1992). The 1971–1991 eruptive activity of Mt. Etna. (First steps to relational data-base realization). *CNR, IIV, Open File Report*, *3/92*, 1–47.

Barberi, F., Brondi, F., Carapezza, M. L., Cavarra, L., & Murgia, C. (2003). Earthen barriers to control lava flows in the 2001 eruption of Mt. Etna. *Journal of Volcanology and Geothermal Research*, *123*, 231–243. https://doi.org/10.1016/S0377-0273(03)00038-6

Barberi, F., Carapezza, M. L., Valenza, M., & Villari, L. (1993). The control of lava flow during the 1991–1992 eruption of Mt. Etna. *Journal of Volcanology and Geothermal Research*, *56*, 1–34. https://doi.org/10.1016/0377-0273(93)90048-V

Bebbington, M. S. (2007). Identifying volcanic regimes using hidden Markov models. *Geophysical Journal International*, *171*, 921–942. https://doi.org/10.1111/j.1365-246x.2007.03559.x

Bebbington, M. S., & Marzocchi, W. (2011). Stochastic models for earthquake triggering of volcanic eruptions. *Journal of Geophysical Research*, *116*, B05204. https://doi.org/10.1029/2010JB008114

Behncke, B., Neri, M., & Nagay, A. (2005). Lava flow hazard at Mount Etna (Italy): New data from a GIS-based study. In M. Manga & G. Ventura (Eds.) *Kinematics and Dynamics of Lava Flows. Special Paper Geological Society of America 396-13* (pp. 187–205). https://doi.org/10.1130/0-8137-2396-5.189

Bell, A. F., La Femina, P. C., Ruiz, M., Amelung, F., Bagnardi, M., Bean, C. J., et al. (2021). Caldera resurgence during the 2018 eruption of Sierra Negra volcano, Galápagos Islands. *Nature Communications*, *12*(1), 1397. https://doi.org/10.1038/s41467-021-21596-4

Bevilacqua, A., Azzaro, R., Branca, S., D'Amico, S., Flandoli, F., & Neri, A. (2021). Modello statistico: Test dipendenza eruzioni/terremoti. Open Report, Product 2a, WP 2. *Task 7, INGV-DPC contract 2019-2021, Att. B2*.

Bevilacqua, A., Bertagnini, A., Pompilio, M., Landi, P., Del Carlo, P., Di Roberto, A., et al. (2020). Major explosions and paroxysms at Stromboli (Italy): A new historical catalog and temporal models of occurrence with uncertainty quantification. *Scientific Reports*, *10*, 17357. https://doi.org/10.1038/s41598-020-74301-8

Bevilacqua, A., Bursik, M., Patra, A., Pitman, E. B., Yang, Q., Sangani, R., & Kobs-Nawotniak, S. (2018). Late Quaternary eruption record and probability of future volcanic eruptions in the Long Valley volcanic region (CA, USA). *Journal of Geophysical Research: Solid Earth*, *123*, 5466–5494. https://doi.org/10.1029/2018JB015644

Bevilacqua, A., Flandoli, F., Neri, A., Isaia, R., & Vitale, S. (2016). Temporal models for the episodic volcanism of Campi Flegrei caldera (Italy) with uncertainty quantification. *Journal of Geophysical Research: Solid Earth*, *121*, 7821–7845. https://doi.org/10.1002/2016JB013171

Bevilacqua, A., Isaia, R., Neri, A., Vitale, S., Aspinall, W. P., Bisson, M., et al. (2015). Quantifying volcanic hazard at Campi Flegrei caldera (Italy) with uncertainty assessment: I. Vent opening maps. *Journal of Geophysical Research: Solid Earth*, *120*, 2309–2329. https://doi.org/10.1002/2014JB011775

Bonaccorso, A., Aoki, Y., & Rivalta, E. (2017). Dike propagation energy balance from deformation modeling and seismic release. *Geophysical Research Letters*, *44*, 5486–5494. https://doi.org/10.1002/2017GL074008

Bonaccorso, A., Bonforte, A., Calvari, S., Del Negro, C., Di Grazia, G., Ganci, G., et al. (2011). The initial phases of the 2008–2009 Mount Etna eruption: A multidisciplinary approach for hazard assessment. *Journal of Geophysical Research*, *116*, B03203. https://doi.org/10.1029/2010JB007906

Bonaccorso, A., Currenti, G., & Del Negro, C. (2013). Interaction of Volcano-tectonic fault with magma storage, intrusion and flank instability: A thirty years study at Mt. Etna volcano. *Journal of Volcanology and Geothermal Research*, *251*, 127–136. https://doi.org/10.1016/j.jvolgeores.2012.06.002

Bonaccorso, A., D'Amico, S., Mattia, M., & Patanè, D. (2004). Intrusive mechanisms at Mt. Etna forerunning the July–August 2001 eruption from seismic and ground deformation data. *Pure and Applied Geophysics*, *161*, 1469–1487. https://doi.org/10.1007/s00024-004-2515-4

Bonaccorso, A., & Giampiccolo, E. (2020). Balance between deformation and seismic energy release: The Dec 2018 'Double-dike' intrusion at Mt. Etna. *Frontiers of Earth Science*, *8*, 583815. https://doi.org/10.3389/feart.2020.583815

Bonforte, A., Bonaccorso, A., Francesco, G., Palano, M., & Puglisi, G. (2008). Feeding system and magma storage beneath Mt. Etna as revealed by recent inflation/deflation cycles. *Journal of Geophysical Research*, *113*, B05406. https://doi.org/10.1029/2007JB005334

Bonforte, A., Branca, S., & Palano, M. (2007). Geometric and kinematic variations along the active Pernicana fault: Implication for the dynamics of Mount Etna NE flank (Italy). *Journal of Volcanology and Geothermal Research*, *160*, 210–222. https://doi.org/10.1016/j.jvolgeores.2006.08.009

Bonforte, A., Guglielmino, F., Coltelli, M., Ferretti, A., & Puglisi, G. (2011). Structural assessment of Mount Etna volcano from Permanent Scatterers analysis. *Geochemistry, Geophysics, Geosystems*, *12*, Q02002. https://doi.org/10.1029/2010GC003213

Boschi, E., Ferrari, G., Gasperini, P., Guidoboni, E., Smriglio, G., & Valensise, G. (1995). *Catalogo dei forti terremoti in Italia dal 461 a.C. al 1980* (p. 973). Ozzano Emilia: ING-SGA.

Boschi, E., Guidoboni, E., Ferrari, G., Mariotti, D., Valensise, G., & Gasperini, P. (2000). Catalogue of strong Italian earthquakes from 461 b.C. to 1997. *Annals of Geophysics*, *43*, 609–868.

Branca, S., & Abate, T. (2019). Current knowledge of Etna's flank eruptions (Italy) occurring over the past 2500 years. From the iconographies of the XVII century to modern geological cartography. *Journal of Volcanology and Geothermal Research*, *385*, 159–178. https://doi.org/10.1016/j.jvolgeores.2017.11.004

Branca, S., Azzaro, R., De Beni, E., Chester, D., & Duncan, A. (2015a). Impacts of 1669eruption and the 1693 earthquakes on the Etna region (eastern Sicily, Italy): An example of recovery and response of a small area to extreme events. *Journal of Volcanology and Geothermal Research*, *303*, 25–40. https://doi.org/10.1016/j.jvolgeores.2015.07.020

Branca, S., Branciforti, M. G., Chiavetta, A. F., & Corsaro, R. A. (2016). The geology of the II century AD amphitheatre area of Catania (Italy): Historical eruptions affecting the urban district. *Geoarchaeology*, *31*, 3–16. https://doi.org/10.1002/gea.21534

Branca, S., & Carlo, P. (2005). Types of eruptions of Etna volcano AD 1670–2003: Implications for short-term eruptive behaviour. *Bulletin of Volcanology*, *67*, 732–742. https://doi.org/10.1007/s00445-005-0412-z

Branca, S., Coltelli, M., Groppelli, G., & Lentini, F. (2011). Geological map of Etna volcano, 1:50,000 scale. *Italian Journal of Geosciences*, *130*(3), 265–291. https://doi.org/10.3301/IJG.2011.15

Branca, S., Condomines, M., & Tanguy, J. C. (2015b). Flank eruptions of Mt Etna during the Greek-Roman and early Medieval periods: New data from ^{226}Ra-^{230}Th dating and archaeomagnetism. *Journal of Volcanology and Geothermal Research*, *304*, 265–271. https://doi.org/10.1016/j.jvolgeores.2015.09.002

Branca, S., De Beni, E., Chester, D., Duncan, A., & Lotteri, A. (2017). The 1928 eruption of Mount Etna (Italy): Reconstructing lava flow evolution and the destruction and recovery of the town of Mascali. *Journal of Volcanology and Geothermal Research*, *335*, 54–70. https://doi.org/10.1016/j.jvolgeores.2017.02.002

Branca, S., De Beni, E., & Proietti, C. (2013). The large and destructive 1669 AD eruption at Etna volcano: Reconstruction of the lava flow field evolution and effusion rate trend. *Bulletin of Volcanology*, *75*, 694. https://doi.org/10.1007/s00445-013-0694-5

Branca, S., & Del Carlo, P. (2004). Eruptions of Mt. Etna during the past 3,200 years: A revised compilation integrating the historical and stratigraphic records. In A. Bonaccorso, S. Calvari, M. Coltelli, C. Del Negro, & S. Falsaperla (Eds.), *Mt. Etna: Volcano Laboratory* (Vol. 143, pp. 1–27). AGU Geophysical Monograph Series. https://doi.org/10.1029/143GM02

Branca, S., & Vigliotti, L. (2015). Finding of an historical document describing an eruption in the NW flank of Etna in July 1643 AD: Timing, location. *Bulletin of Volcanology*, *77*(95), 2–6. https://doi.org/10.1007/s00445-015-0979-y

Brillinger, D. R. (1976). Measuring the association of point processes: A case history. *The American Mathematical Monthly*, *83*, 16–22. https://doi.org/10.1080/00029890.1976.11994027

Calvari, S., Coltelli, M., Neri, M., Pompilio, M., & Scribano, V. (1994). The 1991-93 Etna eruption: Chronology and lava flow-field evolution. *Acta Vulcanologica*, *4*, 1–4. https://doi.org/10.1007/BF00300989

Calvari, S., & Pinkerton, H. (1998). Formation of lava tubes and extensive flow field during the 1991–1993 eruption of Mount Etna. *Journal of Geophysical Research*, *103*(B11), 291–301. https://doi.org/10.1029/97JB03388

Camassi, R., & Stucchi, M. (Eds.) (1997). *NT4.1—A parametric catalogue of damaging earthquakes in the Italian area (release NT4.1.1)* (p. 93). GNDT-CNR Open File Report. Retrieved from http://www.emidius.itim.mi.cnr.it/NT/CONSNT.html

Cannata, A., Di Grazia, G., Montalto, P., Aliotta, M., Patanè, D., & Boschi, E. (2010). Response of Mount Etna to dynamic stresses from distant earthquakes. *Journal of Geophysical Research*, *115*, B12304. https://doi.org/10.1029/2010JB007487

Cappello, A., Bilotta, G., Neri, M., & Del Negro, C. (2013). Probabilistic modeling of future volcanic eruptions at Mount Etna. *Journal of Geophysical Research: Solid Earth*, *118*, 1925–1935. https://doi.org/10.1002/jgrb.50190

Cardaci, C., Falsaperla, S., Gasperini, P., Lombardo, G., Marzocchi, W., & Mulargia, F. (1993). Cross-correlation analysis of seismic and volcanic data at Mt Etna volcano, Italy. *Bulletin of Volcanology*, *55*, 596–603. https://doi.org/10.1007/BF00301812

Caricchi, L., Townsend, M., Rivalta, E., & Namiki, A. (2021). The build-up and triggers of volcanic eruptions. *Nature Reviews Earth & Environment*, *2*, 458–476. https://doi.org/10.1038/s43017-021-00174-8

Carrozzo, M. T., Cosentino, M., Ferlito, A., Giorgetti, F., Patanè, G., & Riuscetti, M. (1975). *Earthquakes catalogue of Calabria and Sicily (1783–1973)* (p. 216). Quaderni Ricerca Scientifica, 93, PFG-CNR

Chen, K., Smith, J. D., Avouac, J. P., Liu, Z., Song, Y. T., & Gualandi, A. (2019). Triggering of the Mw 7.2 Hawaii earthquake of 4 May 2018 by a dike intrusion. *Geophysical Research Letters*, *46*, 2503–2510. https://doi.org/10.1029/2018GL081428

Chesley, C., LaFemina, P. C., Puskas, C., & Kobayashi, D. (2012). The 1707 Mw8.7 Hoei earthquake triggered the largest historical eruption of Mt. Fuji. *Geophysical Research Letters*, *39*, L24309. https://doi.org/10.1029/2012GL053868

Chester, D. K., Duncan, A. M., Guest, J. E., & Kilburn, C. R. J. (1985). *Mount Etna: The anatomy of a volcano* (p. 412). Chapman & Hall.

Conover, W. J. (1980). *Practical nonparametric statistics* (p. 608). John Wiley & Sons.

Cox, D. R. (1955). Some statistical methods connected with series of events. *Journal of the Royal Statistical Society B*, *17*, 129–164. https://doi.org/10.1111/j.2517-6161.1955.tb00188.x

Cox, D. R., & Lewis, P. A. W. (1966). *The statistical analysis of series of events* (p. 285). Chapman & Hall.

Currenti, G., Solaro, G., Napoli, R., Pepe, A., Bonaccorso, A., Del Negro, C., & Sansosti, E. (2012). Modeling of ALOS and COSMO-SkyMed satellite data at Mt Etna: Implications on relation between seismic activation of the Pernicana fault system and volcanic unrest. *Remote Sensing of Environment*, *125*, 64–72. https://doi.org/10.1016/j.rse.2012.07.008

Daley, D. J., & Vere Jones, D. (2005). *An introduction to the theory of point processes, volume I: Elementary theory and methods* (2nd ed., p. 469). Springer.

Del Negro, C., Cappello, A., Bilotta, G., Ganci, G., Hérault, A., & Zago, V. (2019). Living at the edge of an active volcano: Risk from lava flows on Mt. Etna. *Geological Society of America Bulletin*, *132*(7–8), 1615–1625. https://doi.org/10.1130/B35290.1

Del Negro, C., Cappello, A., Neri, M., Bilotta, G., Herault, A., & Ganci, G. (2013). Lava flow hazards at Mount Etna: Constraints imposed by eruptive history and numerical simulations. *Scientific Reports*, *3*, 3493. https://doi.org/10.1038/srep03493

De Rubeis, V., Tosi, P., & Vinciguerra, S. (1997). Time clustering properties of seismicity in the Etna region between 1874 and 1913. *Geophysical Research Letters*, *24*(18), 2331–2334. https://doi.org/10.1029/97GL02340

Farías, C., & Basualto, D. (2020). Reactivating and calming volcanoes: The 2015 MW 8.3 Illapel megathrust strike. *Geophysical Research Letters*, *47*, e2020GL087738. https://doi.org/10.1029/2020GL087738

Favalli, M., Tarquini, S., Fornaciai, A., & Boschi, E. (2009). A new approach to risk assessment of lava flow at Mount Etna. *Geology*, *37*(12), 1111–1114. https://doi.org/10.1130/G30187A.1

Gasperini, P., Gresta, S., & Mulargia, F. (1990). Statistical analysis of seismic and eruptive activities at Mt. Etna during 1978–1987. *Journal of Volcanology and Geothermal Research*, *40*, 317–325. https://doi.org/10.1016/0377-0273(90)90111-r

González, G., Fujita, E., Shibazaki, B., Hayashida, T., Chiodini, G., Lucchi, F., et al. (2021). Increment in the volcanic unrest and number of eruptions after the 2012 large earthquakes sequence in Central America. *Scientific Reports*, *11*, 22417. https://doi.org/10.1038/s41598-021-01725-1

Gresta, G., Marzocchi, W., & Mulargia, F. (1994). Is there a correlation between larger local earthquakes and the end of eruptions at Mount Etna volcano, Sicily? *Geophysical Journal International*, *116*, 230–232. https://doi.org/10.1111/j.1365-246x.1994.tb02140.x

Gresta, S., & Longo, V. (1994). An attempt at identifying seismological precursors for flank eruptions at Mt. Etna volcano. *Acta Vulcanologica*, *5*, 187–192.

Grünthal, G. (1998). *European Macroseismic Scale 1998 (EMS-98), Conseil de l'Europe, Cahiers du Centre Européen de Géodynamique et de Séismologie. European Seismological Commission, Subcommission on Engineering Seismology*. Working Group Macroseismic Scale.

Gruppo di Lavoro CPTI. (1999). *Catalogo Parametrico dei Terremoti Italiani, versione 1* (p. 92). Bologna: ING, GNDT, SGA, SSN. Retrieved from https://emidius.mi.ingv.it/CPTI99/. https://doi.org/10.6092/INGV.IT-CPTI99

Hill, D. P., Pollitz, F., & Newhall, C. (2002). Earthquake–volcano interactions. *Physics Today*, *55*, 41–47. https://doi.org/10.1063/1.1535006

Ho, C. H. (1991). Nonhomogeneous Poisson model for volcanic eruptions. *Mathematical Geology*, *23*, 167–173. https://doi.org/10.1007/bf02066293

Ho, C. H. (1992). Statistical control chart for regime identification in volcanic time-series. *Mathematical Geology*, *24*, 775–787. https://doi.org/10.1007/bf00890701

Imbò, G. (1965). *Catalogue of active volcanoes of the world. Part XVIII, Italy*. International Association of Volcanology.

Latora, V., Vinciguerra, S., Bicciato, S., & Kamimura, R. T. (1999). Identifying seismicity patterns leading flank eruptions at Mt. Etna Volcano during 1981–1996. *Geophysical Research Letters*, *26*(14), 2105–2108. https://doi.org/10.1029/1999GL900480

Linde, A., & Sacks, I. (1998). Triggering of volcanic eruptions. *Nature*, *395*, 888–890. https://doi.org/10.1038/27650

Manga, M., & Brodsky, E. (2006). Seismic triggering of eruptions in the far field: Volcanoes and geysers. *Annual Review of Earth and Planetary Sciences*, *34*, 263–291. https://doi.org/10.1146/annurev.earth.34.031405.125125

McGuire, W., Pullen, A., & Saunders, S. (1990). Recent dyke-induced large-scale block movement at Mount Etna and potential slope failure. *Nature*, *343*, 357–359. https://doi.org/10.1038/343357a0

McGuire, W. J., & Pullen, A. D. (1989). Location and orientation of eruptive fissures and feeder-dykes at Mount Etna; influence of gravitational and regional tectonic stress regimes. *Journal of Volcanology and Geothermal Research*, *38*, 325–344. https://doi.org/10.1016/0377-0273(89)90046-2

McGuire, W. J., Saunders, S. J., & Stewart, I. S. (1997). Intra-volcanic rifting at Mount Etna in the context of regional tectonics. *Acta Vulcanologica*, *9*(1/2), 147–156.

Morley, S. K., & Freeman, M. P. (2007). On the association between northward turnings of the interplanetary magnetic field and substorm onsets. *Geophysical Research Letters*, *34*, L08104. https://doi.org/10.1029/2006GL028891

Mulargia, F. (1992). Time association between series of geophysical events. *Physics of the Earth and Planetary Interiors*, *71*, 147–153. https://doi.org/10.1016/0031-9201(92)90072-4

Mulargia, F., Gasperini, P., & Marzocchi, W. (1991). Pattern recognition applied to volcanic activity: Identification of the precursory patterns to Etna recent flank eruptions and periods of rest. *Journal of Volcanology and Geothermal Research*, *45*, 187–196. https://doi.org/10.1016/0377-0273(91)90058-8

Mulargia, F., Gasperini, P., & Tinti, S. (1987). Identifying different regimes in eruptive activity: An application to Etna volcano. *Journal of Volcanology and Geothermal Research*, *34*, 89–106. https://doi.org/10.1016/0377-0273(87)90095-3

Mulargia, F., Marzocchi, W., & Gasperini, P. (1992). Statistical identification of physical patterns which accompany eruptive activity on Mount Etna, Sicily. *Journal of Volcanology and Geothermal Research*, *53*, 289–296. https://doi.org/10.1016/0377-0273(92)90087-t

Mulargia, F., Tinti, S., & Boschi, E. (1985). A statistical analysis of flank eruptions on Etna volcano. *Journal of Volcanology and Geothermal Research*, *23*, 263–272. https://doi.org/10.1016/0377-0273(85)90037-x

Musson, R., Grünthal, G., & Stucchi, M. (2009). The comparison of macroseismic intensity scales. *Journal of Seismology*, *14*, 413–428. https://doi.org/10.1007/s10950-009-9172-0

Namiki, A., Rivalta, E., Woith, H., Willey, T., Parolai, S., & Walter, T. R. (2019). Volcanic activities triggered or inhibited by resonance of volcanic edifices to large earthquakes. *Geology*, *47*, 67–70. https://doi.org/10.1130/G45323.1

Nercessian, A., Hirn, A., & Sapin, M. (1991). A correlation between earthquakes and eruptive phases at Mt. Etna: An example and past occurrences. *Geophysical Journal International*, *105*, 131–138. https://doi.org/10.1111/j.1365-246x.1991.tb03449.x

Neri, M., Acocella, V., & Behncke, B. (2004). The role of the Pernicana fault system in the spreading of Mount Etna (Italy) during the 2002–2003 eruption. *Bulletin of Volcanology*, *66*, 417–430. https://doi.org/10.1007/s00445-003-0322-x

Neri, M., Acocella, V., Behncke, B., Giammanco, S., Mazzarini, F., & Rust, D. (2011). Structural analysis of the eruptive fissures at Mount Etna (Italy). *Annals of Geophysics*, *54*(5), 464–479. https://doi.org/10.4401/ag-5332

Neri, M., Acocella, V., Behncke, B., Maiolino, V., Ursino, A., & Velardita, R. (2005). Contrasting triggering mechanisms of the 2001 and 2002–2003 eruptions of Mount Etna (Italy. *Journal of Volcanology and Geothermal Research*, *144*, 235–255. https://doi.org/10.1016/j.jvolgeores.2004.11.025

Niehof, J. T., & Morley, S. K. (2012). *Determining the significance of associations between two series of discrete events: Bootstrap methods*. Open Report, LA-14454-MS. Los Alamos National Laboratory. https://doi.org/10.2172/1035497

Nishimura, T. (2017). Triggering of volcanic eruptions by large earthquakes. *Geophysical Research Letters*, *44*, 7750–7756. https://doi.org/10.1002/2017GL074579

Nishimura, T. (2018). Interaction between moderate earthquakes and volcanic eruptions: Analyses of global data catalog. *Geophysical Research Letters*, *45*, 8199–8204. https://doi.org/10.1029/2018GL079060

Patrick, M. R., Houghton, B. F., Anderson, K. R., Poland, M. P., Montgomery-Brown, E., Johanson, I., et al. (2020). The cascading origin of the 2018 Kīlauea eruption and implications for future forecasting. *Nature Communications*, *11*(1), 5646. https://doi.org/10.1038/s41467-020-19190-1

Postpischl, D. (Ed.) (1985). *Catalogo dei terremoti italiani dall' anno 1000 al 1980* (Vol. 114(2B), pp. 1–239). Bologna: Quaderni Ricerca Scientifica. Retrieved from https://emidius.mi.ingv.it/ASMI/study/POST985

Romano, R., & Sturiale, C. (1982). The historical eruptions of Mt. Etna (volcanological data). *Memorie Società Geologica Italiana*, *23*, 75–97.

Rovida, A., Locati, M., Camassi, R., Lolli, B., & Gasperini, P. (2020). The Italian earthquake catalogue CPTI15. *Bulletin of Earthquake Engineering*, *18*, 2953–2984. https://doi.org/10.1007/s10518-020-00818-y

Ruch, J., Pepe, S., Casu, F., Solaro, G., Pepe, A., Acocella, V., et al. (2013). Seismo-tectonic behavior of the Pernicana fault system (Mt Etna): A gauge for volcano flank instability? *Journal of Geophysical Research: Solid Earth*, *118*, 4398–4409. https://doi.org/10.1002/jgrb.50281

Salvi, F., Scandone, R., & Palma, C. (2006). Statistical analysis of the historical activity of Mount Etna, aimed at the evaluation of volcanic hazard. *Journal of Volcanology and Geothermal Research*, *154*, 159–168. https://doi.org/10.1016/j.jvolgeores.2006.01.002

Sandri, S., Marzocchi, W., & Gasperini, P. (2005). Some insights on the occurrence of recent volcanic eruptions of Mount Etna volcano (Sicily, Italy). *Geophysical Journal International*, *163*, 1203–1218. https://doi.org/10.1111/j.1365-246x.2005.02757.x

Sawi, T. M., & Manga, M. (2018). Revisiting short-term earthquake triggered volcanism. *Bulletin of Volcanology*, *80*(7), 57. https://doi.org/10.1007/s00445-018-1232-2

Scarpa, R., Patané, G., & Lombardo, G. (1983). Space-time evolution of seismic activity at Mount Etna during 1974–1982. *Annals of Geophysics*, *1*, 451–462.

Seropian, G., Kennedy, B. M., Walter, T. R., Ichihara, M., & Jolly, A. D. (2021). A review framework of how earthquakes trigger volcanic eruptions. *Nature Communications*, *12*(1), 1004. https://doi.org/10.1038/s41467-021-21166-8

Sharp, A. D. L., Lombardo, G., & Davis, P. M. (1981). Correlation between eruptions of Mount Etna, Sicily, and regional earthquakes as seen in historical records from AD 1582. *Geophysical Journal of the Royal Astronomical Society*, *65*, 507–523. https://doi.org/10.1111/j.1365-246x.1981.tb02726.x

Simkin, T., Siebert, L., McClelland, L., Bridge, D., Newhall, C., & Latter, J. H. (1981). *Volcanoes of the world* (p. 232). John Wiley & Sons.

Smethurst, L., James, M. R., Pinkerton, H., & Tawn, J. A. (2009). A statistical analysis of eruptive activity on Mount Etna, Sicily. *Geophysical Journal International*, *179*(1), 655–666. https://doi.org/10.1111/j.1365-246X.2009.04286.x

Tanguy, J. C. (1981). Les éruptions historiques de l'Etna: Chronologie et localisation. *Bulletin of Volcanology*, *44*(3), 585–640. https://doi.org/10.1007/bf02600588

Tanguy, J. C., Condomines, M., Branca, S., La Delfa, S., & Coltelli, M. (2012). New archeomagnetic and ^{226}Ra-^{230}Th dating of recent lavas for the Geological map of Etna volcano. *Italian Journal of Geosciences*, *131*(2), 241–257. https://doi.org/10.3301/IJG.2012.01

Tanguy, J. C., Condomines, M., Le Goff, M., Chillemi, V., Le Delfa, S., & Patane, G. (2007). Mount Etna eruptions of the last 2,750 years: Revised chronology and location through archeomagnetic and ^{226}Ra-^{230}Th dating. *Bulletin of Volcanology*, *70*, 55–83. https://doi.org/10.1007/s00445-007-0121-x

Vinciguerra, S., Latora, V., Bicciato, S., & Kamimura, R. T. (2001). Identifying and discriminating seismic patterns leading flank eruptions at Mt. Etna volcano during 1981–1996. *Journal of Volcanology and Geothermal Research*, *106*, 211–228. https://doi.org/10.1016/s0377-0273(00)00274-2

Wadge, G. (1977). The storage and release of magma on Mount Etna. *Journal of Volcanology and Geothermal Research*, *2*, 361–384. https://doi.org/10.1016/0377-0273(77)90021-x

Walter, T. R. (2007). How a tectonic earthquake may wake up volcanoes: Stress transfer during the 1996 earthquake–eruption sequence at the Karymsky Volcanic Group, Kamchatka. *Earth and Planetary Science Letters*, *264*(3–4), 347–359. https://doi.org/10.1016/j.epsl.2007.09.006

Wickman, F. E. (1976). Markov models of repose-period patterns of volcanoes. In D. F. Merriam (Ed.), *Random processes in volcanology* (pp. 135–161). Springer-Verlag. https://doi.org/10.1007/978-3-642-66146-4_11